



Geochronological and geochemical characteristics of the Dehzaman intrusive and volcanic rocks (NE Iran): Implication for a Cadomian magmatism

Hossein Hajimirzajan ¹, Azadeh Malekzadeh Shafaroudi ^{2,*}, Seyed Masoud Homam ¹, Mohamad Reza Hidarian Shahri ¹, José Francisco Santos ³

¹ Department of Geology, Faculty of Science, Ferdowsi University of Mashhad, Mashhad, Iran

² Department of Geology and Research Center for Ore Deposit of Eastern Iran, Faculty of Science, Ferdowsi University of Mashhad, Mashhad, Iran

³ Department of Geosciences, Geobiotec Research unit, University of Aveiro, 3810-193 Aveiro, Portugal

ARTICLE INFO

Submitted: August 2018

Accepted: January 2019

Available on line: January 2019

* Corresponding author:
Shafaroudi@um.ac.ir

DOI: 10.2451/2019PM812

How to cite this article:
Hajimirzajan H. et al. (2019)
Period. Mineral. 88, 33-56

ABSTRACT

Cadomian magmatism is interpreted to indicate fragments of late Neoproterozoic-early Cambrian continental arcs bordering the northern margin of Gondwana. Cadomian rocks constitute the main elements of the continental crust of central Iranian block (including the Lut block). An example of such Cadomian rocks from NE Iran is studied here: the Dehzaman igneous rocks within the Kashmar- Kerman Tectonic Zone (KKTZ). The Cadomian exposure in NE Iran includes intrusive rocks with a thick sequence of felsic volcanic rocks. Zircon U-Pb dating of syenogranites and rhyolites yielded ²³⁸U/²⁰⁶Pb crystallization ages of ~521.3 to ~524.3 Ma, respectively and the age of 557 Ma to Biosyenogranites already was obtained by Rossetti et al. (2015) (Ediacaran-Early Cambrian). Geochemically, the intrusive rocks are mostly characterized by high-K content and are similar to the I-type granites. These rocks are characterized by enrichment in large ion lithophile elements (LILEs) and light rare earth elements (LREEs) along with depletion in high field strength elements (HFSEs). Their initial εNd (t) ranges from -0.6 to -2.1 at ⁸⁶Sr/⁸⁷Sr (i)=0.7045-0.7073. The Cadomian rocks from NE Iran, along with similar-aged rocks from Turkey and Iran are suggested to form in an early stage of an active continental margin.

Keywords: Cadomian magmatism; Zircon U-Pb ages; Active continental margin; Gondwana; Iran.

INTRODUCTION

Gondwana was assembled by the collision of about 7-8 Australia-sized Neoproterozoic continents during two main periods, first at ~650-600 Ma and secondly at ~570-520 Ma (Collins and Pisarevsky, 2005). The Neoproterozoic-Cambrian time was dominated by the growth of the Gondwana Supercontinent, resulted from a long-lasting history of orogenic construction, with the final amalgamation during the Cambrian time (Dalziel, 1991; Boger and Miller, 2004; Collins and Pisarevsky, 2005; Cawood, 2005; Cawood and Buchan, 2007; Li et

al., 2008; Torsvik and Cocks, 2013; Nance et al., 2014).

Ediacaran-Cambrian (Cadomian) magmatism is suggested to reflect widespread continental arc magmatism along the northern margin of Gondwana (Ramezani and Tucker, 2003; Ustaömer et al., 2009, 2011; Moghadam et al., 2015). Fragments of the Cadomian crust, rifted away from Gondwana during Cambrian-Ordovician and accreted to Eurasia sequentially, throughout the Phanerozoic time (Stampfli et al., 2002; Murphy et al., 2004; Nance et al., 2008, 2010; Ustaömer et al., 2011).

Occurrence of voluminous Cadomian subduction-

related magmatism in the basement terranes from Iberia, Bohemia, Anatolia to Iran and even Lhasa attests for the formation of an Andean-type active continental margin along the northern margin of the Gondwana Supercontinent (Ramezani and Tucker, 2003; Cawood and Buchan, 2007; Hassanzadeh et al., 2008; Horton et al., 2008; Ustaömer et al., 2009; Saki, 2010; Azizi et al., 2011; Mahmoud et al., 2011; Zhu et al., 2012; Hu et al., 2013; Jamshidi Badr et al., 2013; Rossetti et al., 2015; Shafaii Moghadam et al., 2015). The Cadomian magmatism seems to start from ~600 Ma and continued until 500 Ma with a magmatic “flare-up” at 572 to 528 Ma (Shafaii Moghadam et al., 2017).

Recent efforts to understand the Cadomian exposures in Turkey and Iran emphasize the use of detrital zircons for dating of the igneous rocks, and for their metamorphic equivalents and provenance analysis of Palaeozoic sedimentary units (Ramezani and Tucker, 2003; Hassanzadeh et al., 2008; Ustaömer et al., 2009, 2011, 2012; Jamshidi Badr et al., 2013; Monazzami Bagherzadeh et al., 2015). Bulk rock Sr-Nd data can also provide useful tools for understanding the mechanisms that were involved during the Cadomian magma generation.

According to the recent U-Pb geochronological survey, Cadomian magmatism seems to be widespread in Iran, and can be traced from Alborz (N Iran), Sanandaj-Sirjan Zone, and NE-central Iran including the Kashmar-Kerman Tectonic zone (KKTZ) (Figure 1). The Cadomian magmatism shows a subduction-related magmatism, the occurrence of I-type granitoids is widespread in the Cadomian terranes (e.g., Jamshidi Badr et al., 2013; Alaminia et al., 2013). Although, S-type bodies are reported at the Bornaward area in NE Iran with zircon U-Pb ages of 540 to 550 Ma (magmatic age). Monazzami Bagherzadeh et al. (2015) believe the Bornaward complex were originated from the continental crust. The melt of Bornaward S-type units was derived from psammite and greywacke rocks (Monazzami Bagherzadeh et al., 2015).

The Dehzaman Cadomian intrusions are located in the Central Iranian Block (CIB), in NE Iran. The CIB consists, from east to west, of three major crustal domains: the Lut Block, Tabas Block and the Yazd Block (Berberian and King, 1981). Tabas and Yazd blocks are separated by a nearly 600 km long, arcuate and structurally complex shear zone, the Kashmar-Kerman Tectonic Zone (Ramezani and Tucker, 2003). Variably deformed supracrustal rocks were tilted and exhumed within the KKTZ. The Cadomian magmatic rocks, studied here, outcrop in the NE edge of the KKTZ (Figure 1). The KKTZ provides remarkable exposures of the deeper sections of the CIB, among which the late Neoproterozoic and lower Palaeozoic rocks are abundant

(Stocklin and Setudehnia, 1977; Ramezani and Tucker, 2003). We have focused on geochemistry, Sr-Nd isotope studies and U-Pb zircon geochronology of two different granites in the Dehzaman (NE Iran) with the aim to unravel the age and geochemistry of the meta-igneous rocks from the CIB. This approach helped to understand the crustal growth and reworking mechanism of the Iran crust. We also present new zircon U-Pb age results for the Dehzaman volcanic rocks to better constrain the age of the magmatism in the Iranian Cadomia. These data will be used to strength our understanding about the Cadomian magmatism in Iran and surrounding areas.

GEOLOGICAL SETTING

Cadomian rocks are widespread in NE Iran, especially within the KKTZ. One of the main outcrops of these rocks is the Kuh-e-Sarhangi region that Dehzaman prospect area is located within it. Below, we describe these two areas in more detail.

Kuh-e-Sarhangi region

Kuh-e-Sarhangi, at the northern edge of the KKTZ, includes thick sequence (>2000m) of the variably-metamorphosed Cadomian rocks (Sahandi et al., 2011; Nozaem et al., 2013). These rocks comprise: (i) low-grade metamorphic rocks (slates and phyllites) in N and W of Kale-Abdolghari and Deh Namak villages; (ii) medium-grade metamorphic rocks (mica-, garnet-schists) that are mostly exposed at the W of Klidanak and S-SW of Zeber-Kuh villages; (iii) the Cadomian platform deposits including the recrystallized dolomites of the Soltanieh Formation (Stocklin et al., 1964; Jafari et al., 2007); and (iv) the Zeber-Kuh Formation comprising recrystallized dolomites, marbles, and quartzites (Figure 2). Granitoidic intrusions crosscut the metamorphic rocks (units i and ii). Zircon U-Pb geochronology for some of these intrusions shows Cadomian crystallization ages (ca. 575-535 Ma) (Rossetti et al., 2015). Sahandi et al. (2011) suggested that the igneous and metamorphic rocks have been deformed during a late Neoproterozoic orogeny and exhumed to the upper levels during the Mesozoic and Cenozoic extensional phases.

The Cadomian magmatic and metamorphic rocks are covered by a series of sedimentary rocks including: (i) the Paleozoic (Silurian-Permian) weakly metamorphosed shales, limestones, sandstones, marls, and dolomites; (ii) Mesozoic sediments including shales, sandstones, conglomerates, limestones, and marls.

Dehzaman area

The oldest rocks within the Dehzaman area are slates, phyllites and recrystallized dolomitic limestones. Detailed field investigations reveal three groups of intrusive and

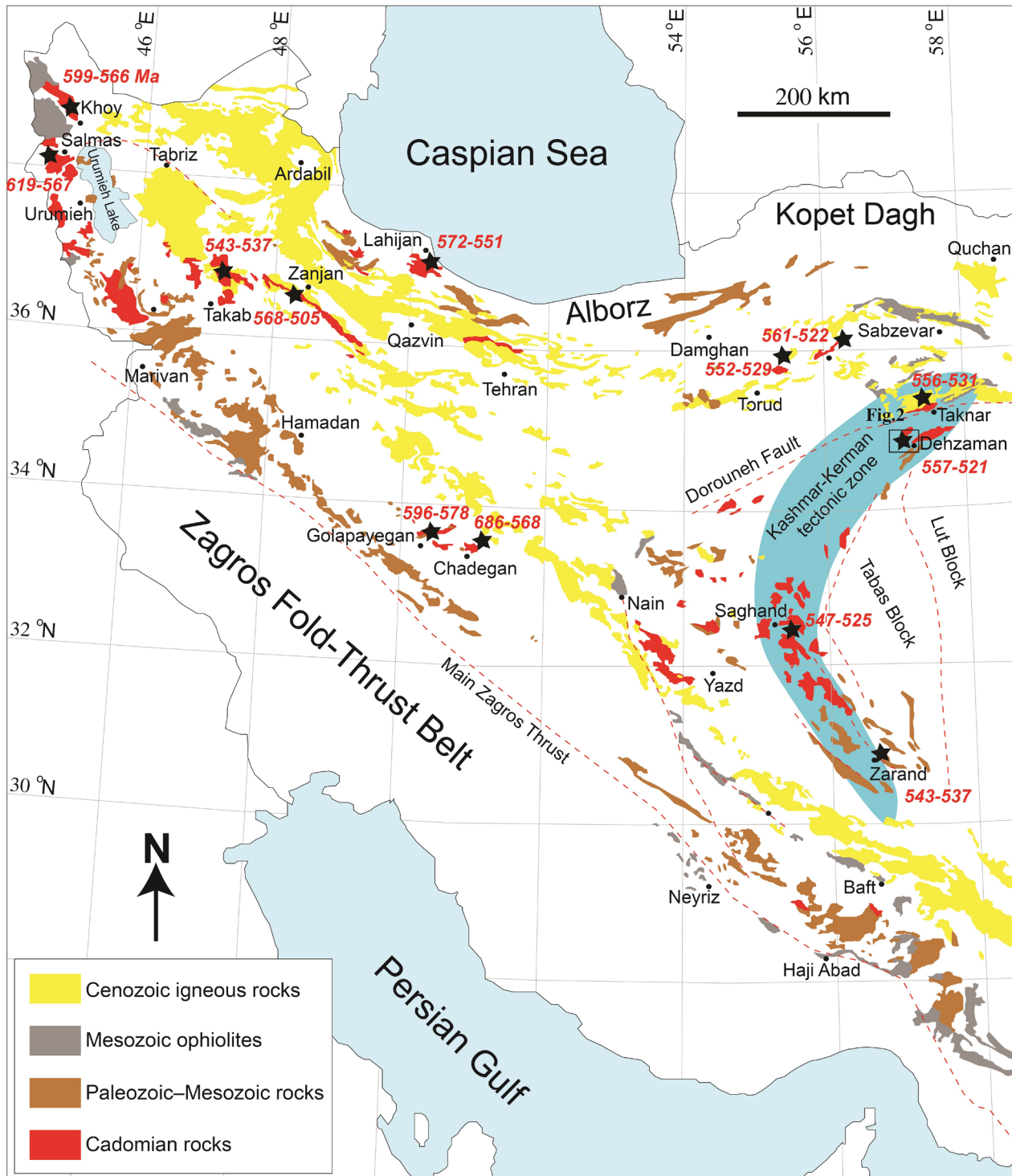


Figure 1. Simplified geological map of Iran (modified after Shafaii Moghadam et al., 2015), with emphasis on the distribution of Cadomian exposures, Mesozoic ophiolites and Eocene magmatic rocks.

volcanic rocks in the Dehzaman area, which include (biotite-bearing) syenogranites, (mylonitic) gneissic granites and rhyolites- rhyodacites.

Biotite syenogranites are widespread in N and central parts of the Dehzaman and make the main rock lithology among the Cadomian rocks (Figure 3). These rocks cover

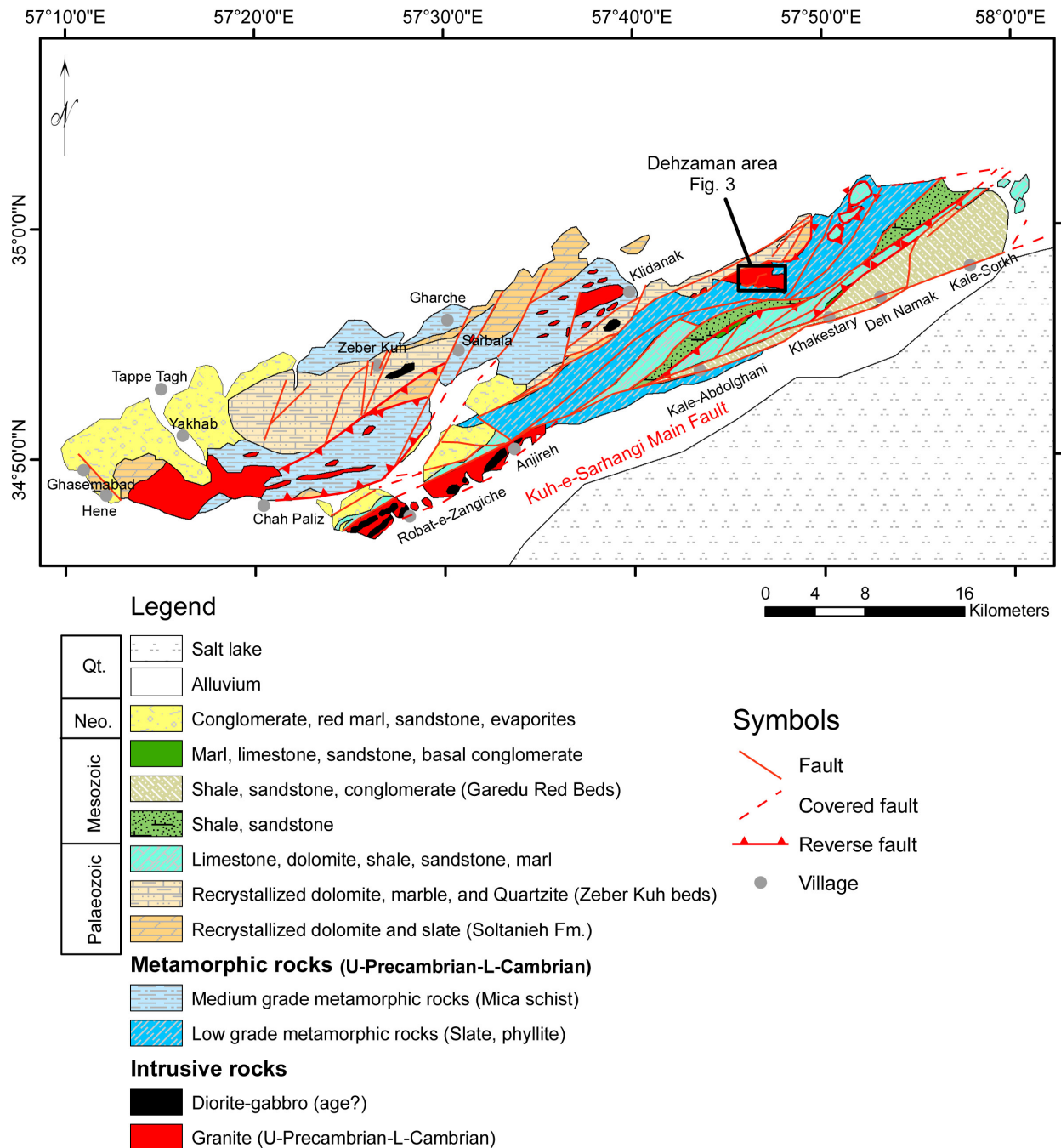


Figure 2. Simplified geological map of the Kuh-e-Sarhangi region (modified after Nozaem et al., 2013). Rectangle shows the location of the Dehzman area.

an area of ~ 5 km².

Gneissic granites occur predominantly in W and E of Dehzman (Figure 3). The mineralogy of gneissic granites is similar to biotite syenogranite, but with more plagioclase crystals. Quartz shows stretching lineation in gneissic granites.

Volcanic rocks in the Dehzman include rhyolites and

rhyodacites. These rocks cover the intrusive rocks in some outcrops. Volcanic rocks show porphyritic, locally mylonitic, texture (Figure 3).

ANALYTICAL METHODS

We sampled different volcanic and plutonic rocks during a detailed field work. We have tried to select

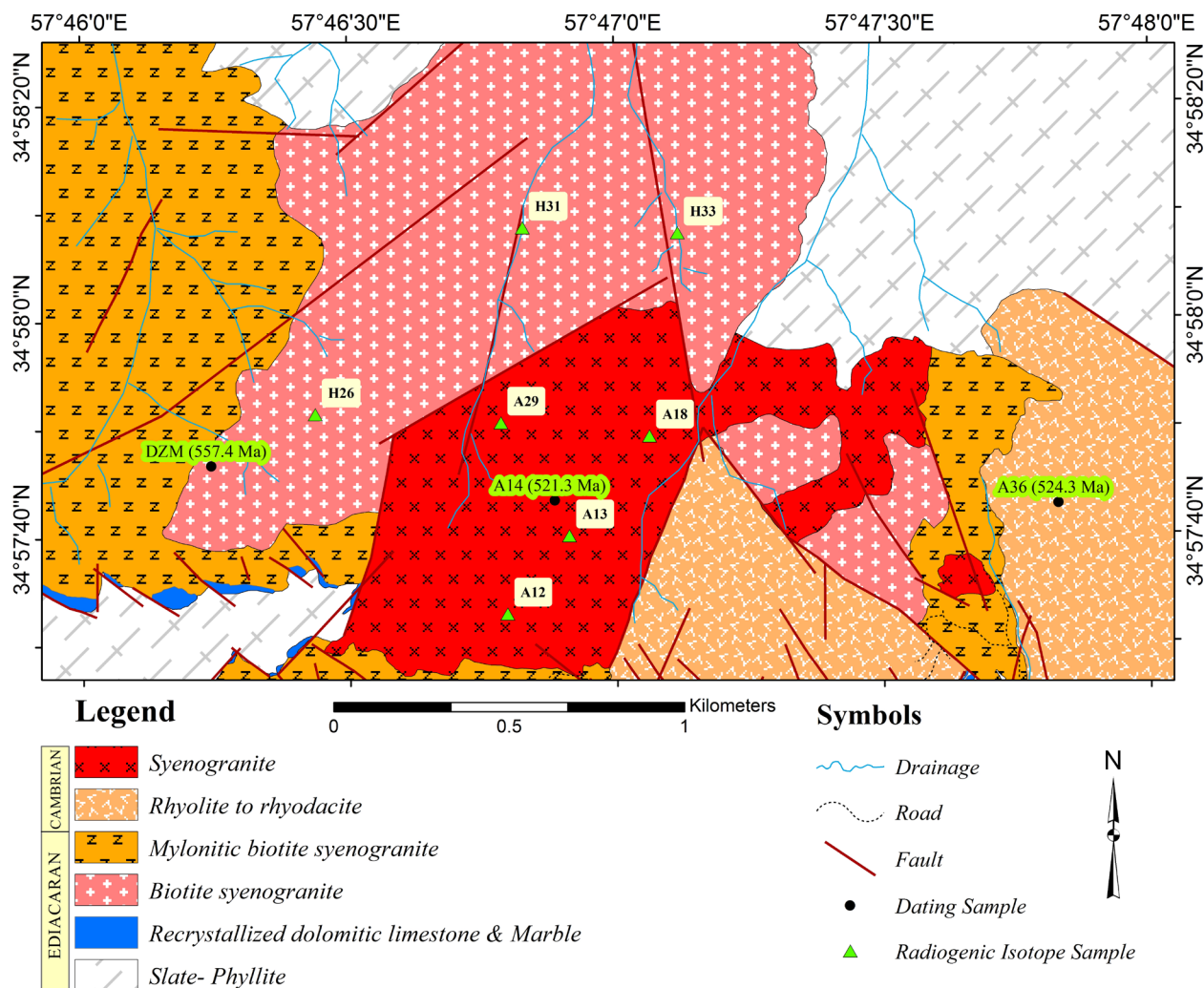


Figure 3. Geological map of the Dehzaman area, with emphasis on the location of collected samples for dating and isotope analysis. Zircon U-Pb age for sample DZM is from Rossetti et al. (2015).

least-altered samples of biotite syenogranites and syenogranites for geochemistry. Two types of different rocks (syenogranites and rhyolites) have been chosen for zircon U-Pb geochronology.

Major and trace elements geochemistry

All samples were crushed after removal of weathered surfaces. The small rock chips were then pulverized in an agate mortar to a grain size of <200 mesh. Major elements compositions of fused disks were analysed by X-ray fluorescence spectrometry (XRF) method at the laboratory of Amethyst, Mashhad, Iran. Trace elements and REE analyses were determined by inductively coupled plasma mass spectrometry (ICP-MS) in the ACME Analytical Laboratories (Vancouver) Ltd.,

Canada. Powdered samples (0.2 g) were fused with lithium metaborate/tetraborate flux and digested by nitric acid before determination by ICP-MS.

Zircon U-Pb geochronology

Two representative rock samples from syenogranite (A-14) and rhyolite (A-36) were chosen for zircon U-Pb dating. Zircons were separated using the convenient methods and mounted along with the appropriate zircon standards, in a 2.5 cm epoxy mount. Zircon U-Pb isotope data were collected by using a New Wave 193 nm ArF laser ablation system coupled to a Nu Plasma HR inductively coupled plasma-mass spectrometer (ICP-MS) at the Arizona Laserchron Centre according to the method described by Gehrels et al. (2008) (for additional information, see

<http://www.sites.google.com/a/laserchron.org/laserchron/>). Uncertainties for reported ^{238}U - ^{206}Pb ages are ~1-2% (2σ) and include both a systematic error (typically ~1-2%), and an error associated with the scatter and precision of a set of measurements for a given sample (~1%, 2σ) (for analytical details see Gehrels et al., 2009). Concordia diagrams were obtained by using the ISOPLOT software (Ludwig, 2003).

Rb-Sr and Sm-Nd isotopic analyses

Sr and Nd isotopic composition were determined at the Laboratório de Geologia Isotópica da Universidade de Aveiro, Portugal. The selected powdered samples were dissolved with HF/HNO₃ in Teflon Parr acid digestion bombs at 200 °C. After evaporation of the final solution, the samples were dissolved with HCl (6 N) and dried down. The elements for analysis were purified using a conventional two-stage ion chromatography technique: (i) separation of Sr and REE elements in ion exchange column with AG8 50 W Bio-Rad cation exchange resin; (ii) purification of Nd from other lanthanide elements in columns with Ln resin (EiChrom Technologies) cation exchange resin. All reagents used in sample preparation were sub-boiling distilled, and pure water was produced by a Milli-Q Element (Millipore) apparatus. Sr was loaded, with H₃PO₄, on a single Ta filament, whereas Nd was loaded, with HCl, on a Ta outer-side filament in a triple filament arrangement. $^{87}\text{Sr}/^{86}\text{Sr}$ and $^{143}\text{Nd}/^{144}\text{Nd}$ isotopic ratios were determined using a Multi-Collector Thermal Ionisation Mass Spectrometer-TIMS-VG Sector 54. Data were obtained in dynamic mode with peak measurements at 1-2 V for ^{88}Sr and 0.5-1 V for ^{144}Nd . Sr and Nd isotopic ratios were corrected for mass fractionation relative to $^{88}\text{Sr}/^{86}\text{Sr}=0.1194$ and $^{146}\text{Nd}/^{144}\text{Nd}=0.7219$. During this study, the SRM-987 standard gave a mean value of $^{87}\text{Sr}/^{86}\text{Sr}=0.710255\pm 23$ (N=10; 95% c.l.) and the JNdi-1 standard yielded $^{143}\text{Nd}/^{144}\text{Nd}=0.5121009\pm 66$ (N=12; 95% c.l.). Initial values of the Nd isotope of samples were calculated according to the procedure of Depaolo, 1981.

PETROGRAPHY

Biotite syenogranites

These rocks show hypidiomorphic granular texture and consist of 50-55 vol% K-feldspar, 8-12 vol% plagioclase (oligoclase), 20-25 vol% quartz, and 6-8 vol% green and brown fine-grained biotite and minor muscovite. Perthites to myrmekitic texture are also usual. Minor zircon, apatite, muscovite and ilmenite are also present (Figure 4A and B). Alkali-feldspars usually occur as megacryst (>5 cm). Orthoclase and plagioclase feldspar are replaced by secondary, alteration-related minerals (<2%) including chlorite, epidote, titanite and sericite (Table 1).

Syenogranites

Syenogranites are medium to coarse grained, with hypidiomorphic granular texture. The mineral assemblages consist of 30-38 vol% quartz, 45-50 vol% K-feldspar and 8-12 vol% plagioclase (Figure 4C and D). Plagioclases generally show kinking and fracturing as the result of tectonic deformation. Apatite, zircon and ilmenite are present as accessory phases (Table 1).

Rhyolites and rhyodacites

These volcanic rocks have a porphyritic texture with a cryptocrystalline to holohyaline groundmass (Figure 4E and F). Euhedral to subhedral phenocrysts consist of K-feldspar (Sanidine), quartz, biotite and rare plagioclase. Zircon and apatite are present as minor components. Due to regional metamorphism and alteration, both plagioclase and K-feldspar have been replaced by epidote and sericite. The glassy groundmass of these rocks shows alteration to chlorite and clay minerals (Table 1).

WHOLE ROCK GEOCHEMISTRY

We have analyzed biotite syenogranites and syenogranites for whole rock major, trace, and rare earth elements (Table 2a and B). Volcanic rocks show higher degree of alteration and therefore we have neglected these samples for whole rock geochemistry.

Intrusive rocks are less altered as testified by their low Loss On Ignition (LOI) values; 0.35-1.01.

Intrusive rocks have quite constant SiO₂ content, ranging from ~74 to 78 wt% (Table 2a and b). Total alkalis (Na₂O+K₂O) are high, 7.67-8.21 wt% in biotite syenogranites and 8.35-9.18 wt% in syenogranites. According to the TAS diagram (Middlemost, 1994), biotite syenogranites and syenogranites plot in the fields of syenogranite and alkali feldspar granite, respectively (Figure 5A). The Dehzaman plutonic rocks have high content of K₂O (from 4.15 to 4.97 wt% in biotite syenogranites and from 3.24 to 7.54 wt% in syenogranites), thereby falling in the high-K calc-alkaline to shoshonitic fields of the K₂O vs SiO₂ diagram by Peccerillo and Taylor (1976) (Figure 5B). Biotite syenogranites are high-K calc-alkaline but syenogranites mostly show shoshonitic signature. Dehzaman granites show peraluminous characteristic, except one sample of biotite syenogranite, which shows metaluminous signature (Figure 5C). In alkali-lime index plot (Na₂O+K₂O+CaO) vs SiO₂ (Frost et al., 2001), syenogranites are mostly calcic-alkali, whereas biotite syenogranites show calc-alkalic signatures (Figure 5D).

In the chondrite-normalized REE diagram (Boynnton, 1984), biotite syenogranites exhibit highly fractionated REE patterns, with strong LREEs enrichment relative to the HREEs ((La/Yb)_N=4.85-13.81), whereas

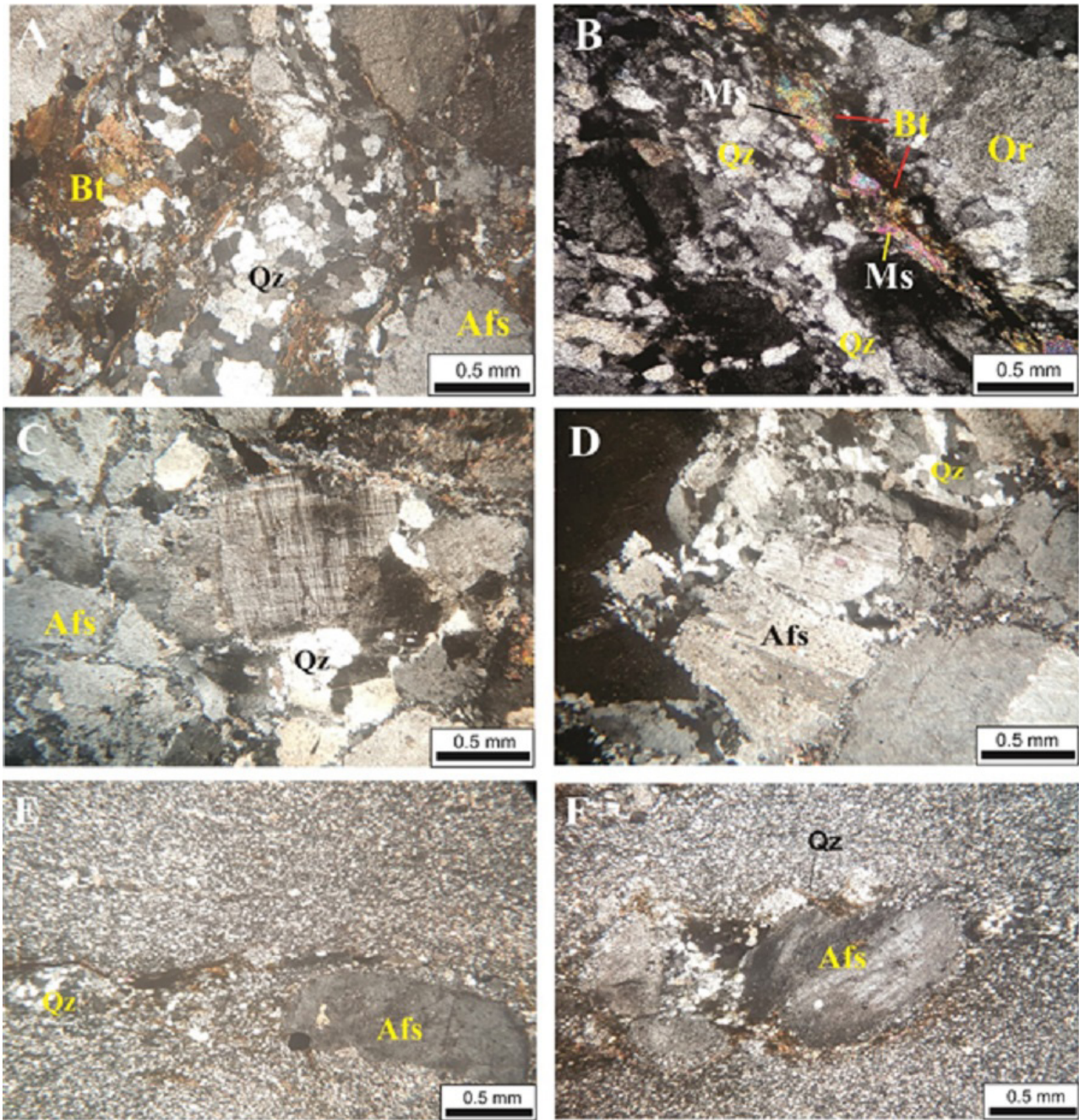


Figure 4. Photomicrographs (XPL) of the Dehzaman granites and volcanic rocks. A and B) Anhedral to subhedral K-feldspar, quartz, and biotite in biotite syenogranites, C and D) Anhedral to subhedral K-feldspar and quartz with hypidiomorphic granular texture in syenogranites, E and F) Rhyolites with porphyritic texture, including quartz and K-feldspar (Afs=K-feldspar, Bt=biotite, Qz=quartz).

syenogranites show fewer fractionated REE patterns than to biotite syenogranites ($(La/Yb)_N=2.02-11.80$). Biotite syenogranites are characterized by negative Eu anomalies ($Eu/Eu^*=0.32-0.58$), whereas syenogranites have both positive and quite negative Eu anomalies ($Eu/Eu^*=0.76-3.85$) (Figure 6A and B).

The primitive mantle-normalized incompatible

elements patterns (Sun and McDonough, 1989) for Dehzaman granites show some significant differences. The samples of biotite syenogranite are more similar and less dispersion than syenogranites. Biotite syenogranites show enrichment in LILEs (such as Cs, Rb, Ba, and K) and depletion in HFSEs (Nb, Ti) relative to the LREEs (Figure 6C). Syenogranite patterns show enrichment in LILEs

Table 1. The main petrographic features of the intrusive and volcanic rocks of Dehzaman area.

Lithology	Texture	Major Mineral	Trace mineral	Alteration
Bt- Syenogranite	hypidiomorphic granular, also Perthites to myrmekitic texture	K-feldspar, plagioclase (oligoclase), quartz, biotite±muscovite	zircon, apatite and ilmenite	Chlorite, epidote, titanite and sericite.
Syenogranite	hypidiomorphic granular	quartz, K-feldspar and plagioclase	Apatite, zircon and ilmenite	Chlorite and less epidote
Rhyolite	Porphyritic with a cryptocrystalline to holohyaline groundmass	K-feldspar (Sanidine), quartz, biotite and rare plagioclase	Zircon and apatite	K-feldspar have been replaced by epidote and sericite, also chlorite and clay minerals

Table 2a. Major, trace, and rare earth elements analyses of biotite syenogranites from the Dehzaman area.

Sample No.	H25	H26	H27	H28	H31	H32	H33	H35
Longitude	E57°46'17.1"	E57°46'26.1"	E57°46'29.8"	E57°46'35.7"	E57°46'49.5"	E57°47'02.9"	E57°47'07.0"	E57°47'16.0"
Latitude	N34°57'51.6"	N34°57'51.4"	N34°57'50.8"	N34°57'51.5"	N34°58'08.5"	N34°58'15.8"	N34°58'08.0"	N34°57'49.8"
	wt%							
SiO ₂	76.25	74.36	74.04	74.21	75.18	76.82	75.62	74.62
TiO ₂	0.08	0.25	0.26	0.28	0.25	0.15	0.2	0.21
Al ₂ O ₃	11.68	12.94	13.33	12.89	12.43	11.96	12.64	12.3
FeOt	1.28	0.91	2.15	2.04	0.84	1.73	0.75	2.54
MnO	0.05	0.03	0.03	0.04	0.05	0.03	0.04	0.13
MgO	0.01	0.45	0.51	0.47	0.41	0.16	0.27	0.38
CaO	1.40	1.00	0.45	0.88	0.88	0.54	0.53	0.65
Na ₂ O	3.24	3.52	3.54	3.27	3.37	3.24	3.44	3.46
K ₂ O	4.97	4.15	4.63	4.74	4.63	4.82	4.60	4.51
P ₂ O ₅	0.02	0.04	0.04	0.05	0.04	0.03	0.03	0.03
L.O.I	0.92	0.83	0.83	0.95	0.51	0.41	0.62	1.01
Total	99.90	98.48	99.81	99.82	98.59	99.89	98.74	99.84
	ppm							
Ba	381	650	883	888	564	377	801	707
Be	5	1	2	2	<1	4	2	4
Co	0.2	2.0	3.2	1.8	2.0	1.4	0.9	2.3
Cs	4.8	1.3	1.1	0.8	2.3	2.0	1.0	1.0
Ga	11.4	13.7	13.7	13.9	13.7	11.8	12.8	14.3
Hf	2.2	4.8	5.5	5.3	5.0	4.2	3.9	5.9
Nb	4.1	6.0	7.0	6.9	6.8	6.2	4.3	7.5
Rb	158.4	117.8	120.8	108.0	139.6	160.5	123.7	119.8
Sn	2	2	2	2	1	2	1	1
Sr	40.0	100.3	164.6	156.2	74.4	53.5	82.1	74.1
Ta	1.0	0.7	0.9	0.6	1.0	1.0	0.6	0.7
Th	18.9	15.6	13.7	13.0	19.7	24.7	17.9	17.3
U	2.2	2.6	2.9	2.5	2.9	3.4	3.7	3.7
V	<8	19	16	18	11	<8	9	14
W	<0.5	1.8	0.8	<0.5	<0.5	0.6	<0.5	1.0
Zr	40.4	151.5	173.2	164.0	140.0	114.1	120.3	178.8
Y	15.6	15.8	17.9	21.9	15.7	16.4	10.5	21.9

Table 2a. Continued ...

Sample No.	H25	H26	H27	H28	H31	H32	H33	H35
Longitude	E57°46'17.1"	E57°46'26.1"	E57°46'29.8"	E57°46'35.7"	E57°46'49.5"	E57°47'02.9"	E57°47'07.0"	E57°47'16.0"
Latitude	N34°57'51.6"	N34°57'51.4"	N34°57'50.8"	N34°57'51.5"	N34°58'08.5"	N34°58'15.8"	N34°58'08.0"	N34°57'49.8"
ppm								
La	18.4	25.8	18.4	17.7	24.9	44.5	23.2	29.9
Ce	32.6	50.1	36.8	36.8	44.7	78.4	39.6	55.7
Pr	3.58	5.55	4.04	4.69	4.83	7.73	4.16	6.02
Nd	12.5	19.9	13.3	18.7	16.1	23.5	12.2	21.2
Sm	2.62	3.60	2.88	4.18	3.08	3.40	1.85	4.25
Eu	0.29	0.51	0.53	0.65	0.42	0.34	0.27	0.48
Gd	2.54	3.27	2.67	4.03	2.78	3.12	1.68	3.77
Tb	0.43	0.51	0.50	0.66	0.47	0.44	0.28	0.62
Dy	2.80	3.29	3.24	4.04	2.82	2.69	1.99	3.75
Ho	0.62	0.60	0.65	0.76	0.54	0.59	0.39	0.86
Er	2.02	2.13	2.08	2.43	1.79	1.92	1.14	2.47
Tm	0.33	0.33	0.32	0.38	0.30	0.30	0.19	0.41
Yb	2.56	2.20	2.39	2.20	2.16	2.22	1.27	2.65
Lu	0.37	0.33	0.36	0.37	0.35	0.38	0.22	0.44
Ratio								
(La/Yb) _N	4.85	7.91	5.19	5.42	7.77	13.51	12.32	7.61
Eu/Eu*	0.34	0.45	0.58	0.48	0.44	0.32	0.47	0.37

Table 2b. Major, trace, and rare earth elements analyses of syenogranites from the Dehzaman area.

Sample No.	H34	A12	A13	A15	A18	A29	A30	A31
Longitude	E57°47'13.9"	E57°46'47.6"	E57°46'54.6"	E57°46'52.6"	E57°47'03.7"	E57°46'47.0"	E57°46'46.1"	E57°46'44.4"
Latitude	N34°57'55.2"	N34°57'32.8"	N34°57'40.0"	N34°57'52.6"	N34°57'49.2"	N34°57'50.5"	N34°57'42.9"	N34°57'37.9"
wt%								
SiO ₂	76.50	75.97	75.99	75.00	75.47	74.36	75.05	76.60
TiO ₂	0.13	0.21	0.25	0.26	0.21	0.95	0.24	0.13
Al ₂ O ₃	12.81	12.94	13.02	13.42	13.6	13.49	12.74	12.68
FeOt	0.92	0.44	0.47	1.24	0.41	1.42	1.22	1.07
MnO	0.02	0.02	0.05	0.03	0.02	0.02	0.03	0.02
MgO	0.00	0.40	0.20	0.04	0.05	0.18	0.52	0.08
CaO	0.46	0.19	0.26	0.27	0.43	0.40	0.48	0.07
Na ₂ O	3.78	3.90	5.24	3.09	4.01	3.53	3.32	1.24
K ₂ O	4.57	4.71	3.24	6.09	4.65	4.93	5.72	7.54
P ₂ O ₅	0.01	0.01	0.01	0.01	0.01	0.01	0.02	0.01
L.O.I	0.61	0.44	0.44	0.36	0.35	0.49	0.51	0.37
Total	99.81	99.23	99.17	99.81	99.21	99.78	99.85	99.81
ppm								
Ba	900	647	542	1191	964	947	864	905
Be	4	4	4	<1	2	4	<1	1
Co	0.6	1.1	0.3	0.4	0.5	0.6	0.8	0.9
Cs	0.3	0.2	0.1	0.2	0.1	0.1	0.2	0.2
Ga	13.7	13.7	14.2	11.7	12.3	10.6	14.5	12.4
Hf	5.4	6.1	6.5	5.9	5.5	5.8	5.9	5.1
Nb	7.0	2.7	4.4	6.0	7.6	20.2	4.5	3.5
Rb	84.1	65.5	49.6	97.0	75.4	78.0	81.7	117.5

Table 2b. Continued ...

Sample No.	H34	A12	A13	A15	A18	A29	A30	A31
Longitude	E57°47'13.9"	E57°46'47.6"	E57°46'54.6"	E57°46'52.6"	E57°47'03.7"	E57°46'47.0"	E57°46'46.1"	E57°46'44.4"
Latitude	N34°57'55.2"	N34°57'32.8"	N34°57'40.0"	N34°57'52.6"	N34°57'49.2"	N34°57'50.5"	N34°57'42.9"	N34°57'37.9"
	wt%							
Sn	1	<1	<1	<1	<1	1	<1	<1
Sr	89.4	57.6	75.6	140.9	145.2	110.8	141.8	121.6
Ta	0.9	0.7	0.9	0.7	0.8	1.2	0.6	0.6
Th	17.5	15.7	25.9	9.1	18.8	23.6	20.5	25.2
U	1.7	0.5	0.8	2.9	2.2	5.7	2.6	2.2
V	<8	<8	<8	<8	<8	<8	<8	<8
W	0.7	1.2	<0.5	<0.5	<0.5	0.8	<0.5	0.5
Zr	155.6	185.0	199.9	184.8	186.6	187.8	176.0	129.5
Y	18.8	2.1	7.3	14.9	8.3	15.0	21.6	14.9
La	15.5	2.9	6.6	16.2	10.8	30.5	35.1	37.8
Ce	26.8	3.8	7.5	20.8	12.8	35.8	38.2	41.2
Pr	2.75	0.28	0.55	1.32	0.84	2.14	2.20	2.57
Nd	9.8	0.9	1.5	3.0	1.9	4.6	4.7	6.5
Sm	2.27	0.18	0.36	0.61	0.41	1.02	1.19	1.25
Eu	0.54	0.22	0.28	0.36	0.31	0.57	0.48	0.48
Gd	2.10	0.17	0.55	1.05	0.66	1.49	2.11	1.71
Tb	0.40	0.04	0.13	0.25	0.14	0.34	0.47	0.34
Dy	2.90	0.30	1.11	2.29	1.09	2.70	3.51	2.48
Ho	0.72	0.10	0.30	0.63	0.29	0.69	0.75	0.54
Er	2.48	0.27	1.01	2.24	1.23	2.39	2.55	1.93
Tm	0.39	0.04	0.15	0.40	0.21	0.40	0.38	0.32
Yb	2.68	0.45	1.12	2.70	1.75	2.98	2.59	2.16
Lu	0.40	0.09	0.21	0.43	0.29	0.50	0.39	0.35
	Ratio							
(La/Yb) _N	3.9	4.34	3.97	4.05	4.16	6.9	9.14	11.8
Eu/Eu*	0.76	3.85	1.92	1.38	1.82	1.41	0.93	1.00

except Cs element. Also, Ba and Sr normalized values are higher than biotite syenogranites, which matches to positive Eu anomaly. Although, depletion in HFSEs is similar to biotite syenogranite patterns (Figure 6D). Generally these features are typical for the subduction-related magmas, such as the calc-alkaline igneous rocks of the active continental margins (Gill, 1981; Pearce and Peate, 1995; Walker et al., 2001; Ma et al., 2014).

U-PB ZIRCON GEOCHRONOLOGY

We have dated two samples from the Dehzaman, including syenogranites and rhyolites. Biotite syenogranites was dated by Rossetti et al. (2015) using in situ U-Pb zircon geochronology, which is interpreted as that of crystallization age. Biotite syenogranites show Concordia age of 557 ± 4 Ma (MSWD=0.47) (Rossetti et al., 2015).

Zircon U-Pb age results for Dehzaman syenogranites and rhyolites are shown in Figure 7 and reported in Table 3a and B.

Rhyolite (sample A-36)

Zircons from sample A-36 are colourless to pale yellow, transparent, and commonly euhedral. The grain size ranges between 50 and 200 μm , with a length/width ratio of 1:1-4:1. They show oscillatory zoning in CL images, which is generally interpreted as typical of magmatic zircons (Connelly, 2001; Corfu et al., 2003). The Th/U ratios of zircons are between 0.7 and 2.3, with an average of 1.5. The relatively high Th/U ratios are consistent with magmatic zircons. Inherited cores are missing in this samples. Fourteen analysed zircons from this sample have concordant $^{206}\text{Pb}/^{238}\text{U}$ and $^{207}\text{Pb}/^{235}\text{U}$ ratios within the analytical precision (Figure 7A and B), Concordia age of 524.3 ± 5.3 Ma (MSWD=0.21). This age (lower Cambrian) is considered as the crystallization age of Dehzaman rhyolites.

Syenogranite (sample A-14)

Zircons from sample A-14 are colourless, transparent,

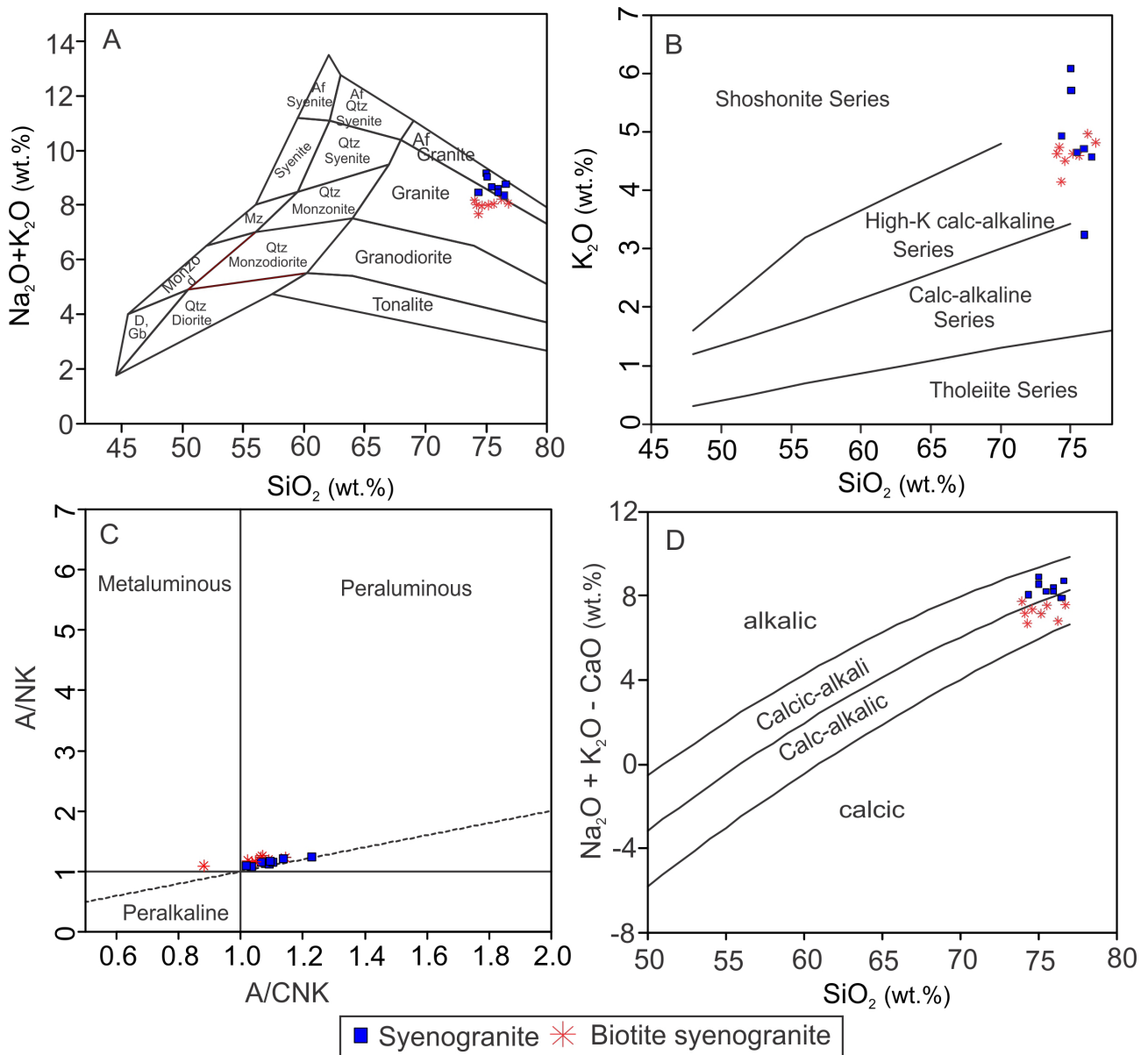


Figure 5. A) Na₂O + K₂O vs SiO₂ classification diagram (Middlemost, 1994) for Dehzaman granitoids, B) K₂O vs SiO₂ discrimination diagram (Peccerillo and Taylor, 1976). The Dehzaman intrusive rocks mostly plot in the high-K calc-alkaline and shoshonite fields, C) A/NK (molar Al₂O₃/Na₂O+K₂O) vs A/CNK (molar Al₂O₃/CaO+Na₂O+K₂O) diagram (Maniar and Piccoli, 1989) for Dehzaman granites, D) Na₂O+K₂O-CaO vs SiO₂ discrimination diagram (Frost et al., 2001) showing the nature of the Dehzaman intrusive rocks. Syenogranites show calcic-alkali signature, whereas biotite syenogranites are calc-alkalic.

and commonly euhedral. Zircon are short to quite prismatic with grain size ranging between 60 and 150 μm . They have a length/width ratio of 1:1-3:1. Zircon show oscillatory zoning in CL images. Th/U ratio of analysed zircons varied between 1.2 and 3.2, with an average of 2.2. Twenty-four analyzed zircons have concordant ²⁰⁶Pb/²³⁸U and ²⁰⁷Pb/²³⁵U ratios within the analytical precision (Figure 7C and D), Concordia age of 521.3 ± 4.2

Ma (MSWD~1). This age (lower Cambrian) is considered as the best crystallization age of the syenogranites.

Our new zircon U-Pb age results show age of 524.3 ± 5.3 Ma for the rhyolite and 521.3 ± 4.2 Ma for the crystallization of syenogranites, therefore rhyolites and syenogranites are coeval. These ages are quite younger than the age of biotite syenogranites (~557 Ma), obtained by Rossetti et al. (2015).

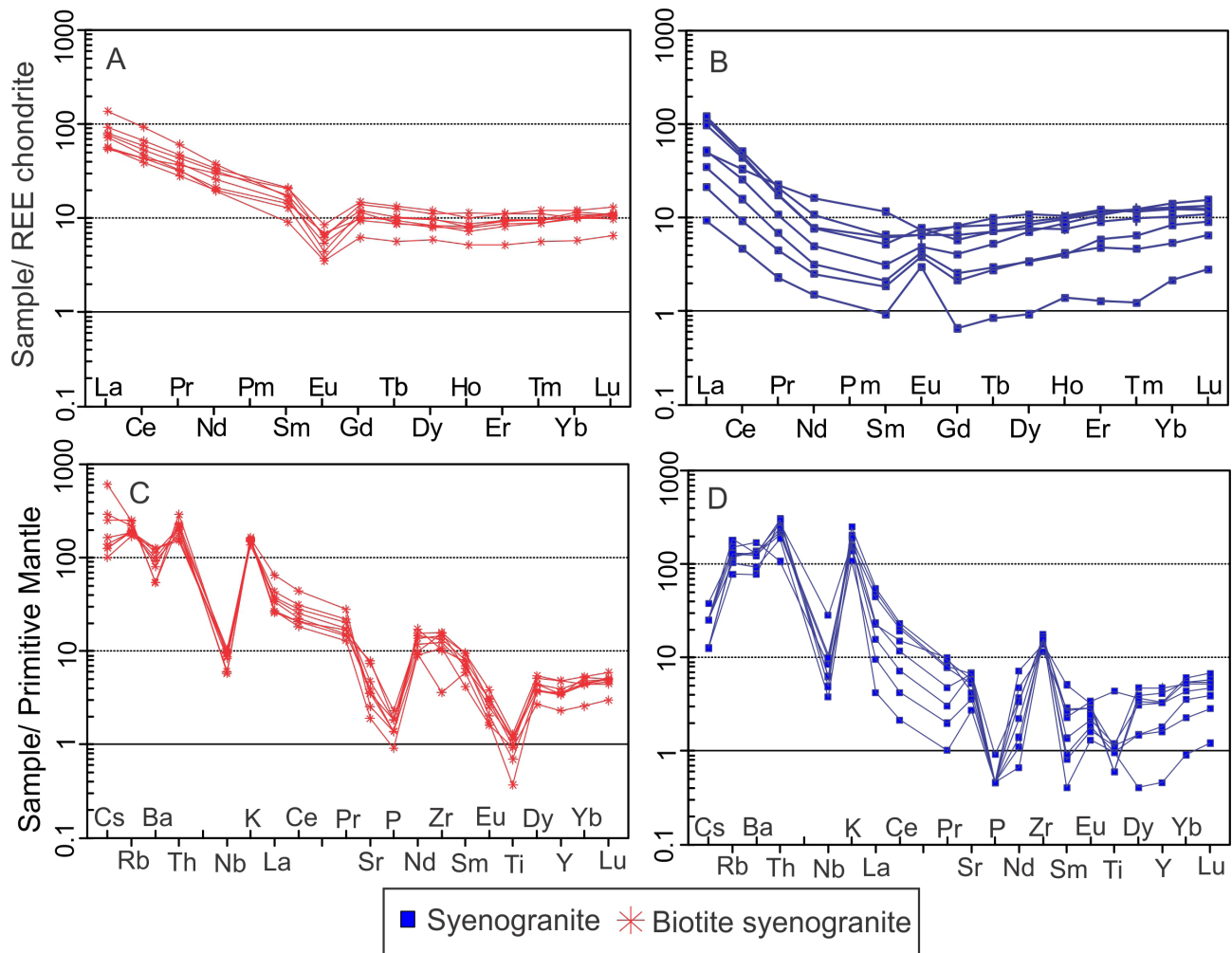


Figure 6. Chondrite-normalized rare earth elements diagram for biotite syenogranites (A) and syenogranites (B). Primitive mantle-normalized trace element patterns for biotite syenogranites (C) and syenogranites (D) [chondrite and primitive mantle abundances are from Boynton (1984) and Sun and McDonough (1989), respectively].

SR-ND ISOTOPE GEOCHEMISTRY

Here, we record $^{87}\text{Sr}/^{86}\text{Sr}$ and $^{143}\text{Nd}/^{144}\text{Nd}$ isotopic ratios and Nd model ages (TDM) for biotite syenogranites (3 samples) and syenogranites (4 samples) (Table 4a and B). Initial $^{87}\text{Sr}/^{86}\text{Sr}$ ratios and Nd epsilon [$\epsilon\text{Nd}(t)$] values are calculated using the crystallization ages of biotite syenogranites (557 Ma) and syenogranites (521 Ma) using the ^{87}Rb decay constant values of Villa et al. (2015).

Biotite syenogranites have initial $^{87}\text{Sr}/^{86}\text{Sr}$ ratios of 0.702834 to 0.705402 whereas their initial $^{143}\text{Nd}/^{144}\text{Nd}$ ratio varies from 0.511881 to 0.511892, with $\epsilon\text{Nd}(t)$ ranging from -0.6 to -0.8. Syenogranites have Sr-Nd isotope compositions which are quite different than those of biotite syenogranites: $(^{87}\text{Sr}/^{86}\text{Sr})_i=0.706694$ to 0.707399, $(^{143}\text{Nd}/^{144}\text{Nd})_i=0.511857$ to 0.511930 and $\epsilon\text{Nd}(t)=-0.7$ to -2.1 (Table 4a and b). The ϵNd values

are partly overlapping between Bt-syenogranites and syenogranites.

In the ϵNd versus initial $^{87}\text{Sr}/^{86}\text{Sr}$ diagram (Figure 8), biotite syenogranites have variable initial $(^{87}\text{Sr}/^{86}\text{Sr})_i$ ratio and plot in the left side of the mantle array. Variable $(^{87}\text{Sr}/^{86}\text{Sr})_i$ of biotite syenogranites could be due to the variable bulk rock Rb/Sr ratio of these rocks. Syenogranites plot to the right of the mantle array, toward the continental upper crust domain.

DISCUSSION

Tectono-magmatic setting

Dehzaman intrusions are characterized by high-K calc-alkaline to shoshonitic signatures. Such rocks are typical of active continental arcs (Pearce and Peate, 1995).

Furthermore, the trace elements-normalized patterns of

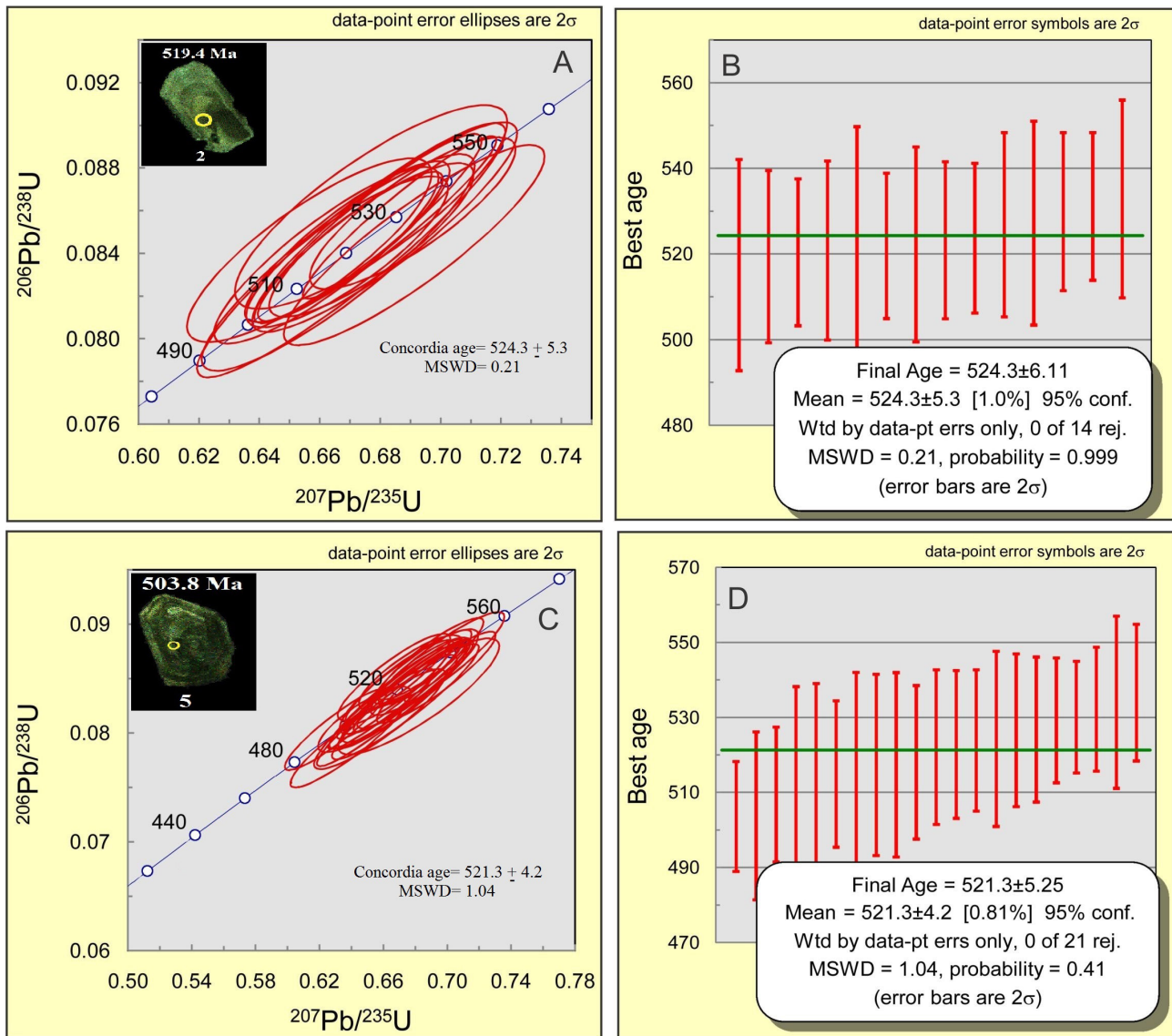


Figure 7. Cathodoluminescence (CL) images of Dehzaman zircons (A and C). Concordia and mean $^{206}\text{Pb}/^{238}\text{U}$ age plots for Dehzaman rhyolite (A and B) and syenogranite (C and D).

the Dehzaman rocks, such as enrichment in LILEs (K, Th, U, Rb) and depletion in the HFSEs (Nb, Ta, Ti) (Figure 6A to D), are indicative of the subduction-related magmatism at convergent margins (Foley et al., 1987; Altherr et al., 2008; Boari et al., 2009). The subduction-related origin of the Dehzaman granites can be further testified by the trace-elements discrimination diagrams (Figure 9). In Rb vs Nb+Y and Rb vs Ta+Yb diagrams (Pearce et al., 1984), the granitic rocks plot in the volcanic arc granitic (VAG) field (Figure 9A and B).

The Th/Yb versus Nb/Yb plot is conventionally used to discriminate between the subduction- and non-subduction-related igneous rocks (Pearce, 2008), with subduction-related magmatic rocks are represented by higher Th/

Yb, but lower Nb/Yb ratios (Figure 9C). In this diagram, the Dehzaman granites show higher Th/Yb values, well within the field of active continental margins (Figure 9C). However contribution of continental crust during magma ascent and assimilation could also increase the Th/Yb ratio. The Dehzaman granites share many similarities, such as high concentrations of incompatible elements and depletion in Nb-Ta along with high Th/Yb ratio, with other Cadomian igneous rocks in Iran (Ramezani and Tucker, 2003; Hassanzadeh et al., 2008; Jamshidi Badr et al., 2013; Alaminia et al., 2013; Shafaii Moghadam et al., 2015) (Figure 9).

Abundance of incompatible elements in granites can be correlated to the degree of arc maturity (Brown et

Table 3a. Zircon U-Pb age results of the Dehzaman rhyolite (sample A-36).

Sample No.	U (ppm)	²⁰⁶ Pb/ ²⁰⁴ Pb	U/Th	²⁰⁶ Pb*/ ²⁰⁷ Pb*	(%)±	²⁰⁷ Pb*/ ²³⁵ U*	(%)±	²⁰⁶ Pb*/ ²³⁸ U	(%)±	Best Age (Ma)	(Ma) ±
1	149	34477	1.4	17.2915	1.2	0.6661	2.8	0.0836	2.5	517.4	12.3
2	420	27730	1.1	17.4643	1.1	0.6622	2.3	0.0839	2.0	519.4	10.1
3	390	32794	1.2	17.3190	1.1	0.6691	2.0	0.0841	1.7	520.4	8.6
4	138	6218	1.8	17.6647	1.4	0.6566	2.5	0.0842	2.1	520.9	10.5
5	179	18589	1.5	17.2993	1.2	0.6704	3.1	0.0842	2.9	520.9	14.5
6	354	69948	1.1	17.3420	0.8	0.6702	1.9	0.0843	1.7	521.9	8.5
7	192	34478	1.4	16.8242	1.2	0.6913	2.6	0.0844	2.3	522.3	11.4
8	264	40313	1.3	17.4142	1.0	0.6691	2.1	0.0846	1.8	523.2	9.2
9	197	45305	2.3	17.2244	1.1	0.6772	2.0	0.0846	1.7	523.7	8.7
10	375	68367	1.4	17.3629	0.8	0.6760	2.3	0.0852	2.1	526.9	10.8
11	148	23912	1.3	17.2340	1.2	0.6816	2.6	0.0852	2.4	527.3	11.9
12	1430	83794	0.7	17.2029	0.6	0.6864	1.9	0.0857	1.8	530.0	9.2
13	190	11255	1.3	17.1352	1.1	0.6908	2.0	0.0859	1.7	531.2	8.6
14	120	12690	1.6	17.5421	1.5	0.6771	2.7	0.0862	2.3	532.9	11.6

Table 3b. Zircon U-Pb age results of the Dehzaman syenogranite (sample A-14).

Sample No.	U (ppm)	²⁰⁶ Pb/ ²⁰⁴ Pb	U/Th	²⁰⁶ Pb*/ ²⁰⁷ Pb*	(%)±	²⁰⁷ Pb*/ ²³⁵ U*	(±%)	²⁰⁶ Pb*/ ²³⁸ U	(%)	Best Age (Ma)	(Ma)±
1	479	31917	1.9	17.0937	0.9	0.6377	2.3	0.0791	2.1	490.7	10.0
2	402	27483	2.0	17.5663	0.8	0.6303	2.1	0.0803	1.9	498.1	9.1
3	381	36051	2.0	17.2775	1.0	0.6482	1.8	0.0813	1.5	503.6	7.3
4	1060	40961	1.2	17.0292	1.1	0.6578	2.6	0.0813	2.3	503.8	11.2
5	285	19109	1.8	17.2037	0.9	0.6589	2.0	0.0822	1.8	509.5	9.0
6	633	25877	1.7	17.0943	0.8	0.6654	2.9	0.0825	2.8	511.2	13.5
7	461	61450	1.4	16.9505	1.0	0.6739	2.8	0.0829	2.6	513.3	12.9
8	616	19447	1.6	17.1038	1.0	0.6701	2.2	0.0832	2.0	514.9	9.7
9	466	9791	1.8	16.8412	1.5	0.6822	3.0	0.0834	2.6	516.2	12.9
10	602	34284	1.9	17.0888	0.8	0.6740	2.6	0.0836	2.4	517.4	12.1
11	655	137836	1.5	17.2493	0.8	0.6677	2.6	0.0836	2.5	517.4	12.3
12	751	105938	1.2	17.3122	0.7	0.6662	2.2	0.0837	2.1	518.1	10.2
13	437	13185	1.5	17.1650	0.7	0.6774	2.2	0.0844	2.1	522.1	10.3
14	279	216507	1.8	17.1461	0.8	0.6791	2.1	0.0845	2.0	522.9	9.9
15	350	98797	1.3	17.4116	0.9	0.6702	2.1	0.0847	1.9	523.9	9.4
16	305	31342	2.4	17.2725	1.2	0.6761	2.6	0.0847	2.3	524.3	11.7
17	375	92725	1.5	16.9255	0.9	0.6931	2.2	0.0851	2.0	526.6	10.2
18	503	11734	1.8	17.6017	1.0	0.6667	2.2	0.0852	1.9	526.8	9.7
19	361	93616	1.7	17.4241	1.0	0.6768	1.9	0.0856	1.6	529.3	8.3
20	437	46681	1.8	17.2266	0.9	0.6857	1.7	0.0857	1.5	530.1	7.5
21	581	79845	3.2	17.3240	0.9	0.6847	1.8	0.0861	1.6	532.2	8.3
22	184	51501	1.8	17.1544	1.0	0.6940	2.5	0.0864	2.2	534.1	11.5
23	349	28490	2.3	17.3479	0.8	0.6897	2.0	0.0868	1.8	536.6	9.1

al., 1984). Simultaneous increase in Nb content and Rb/Zr ratio indicates the enhancement of continental arc maturity. Dehzaman intrusive rocks have quite low Nb content and Rb/Zr ratio in the Nb vs Rb/Zr diagram (Figure 10), attesting the Dehzaman rocks were formed during an earliest stage of subduction in an active arc.

Granites affinity and evolution

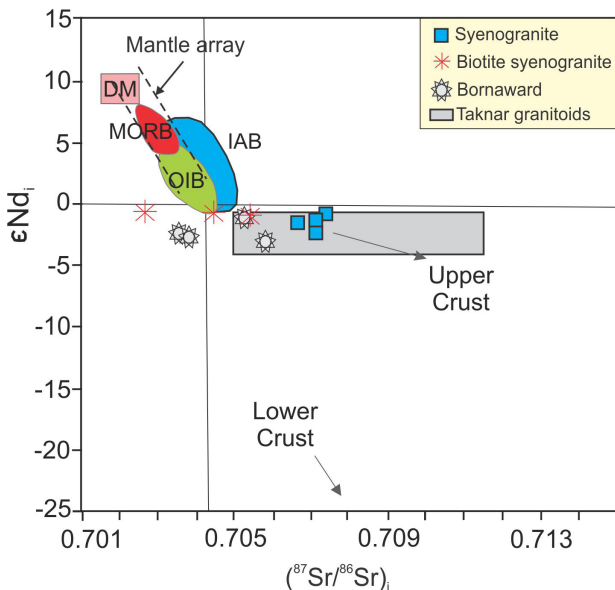
The reported ages of Dehzaman igneous rocks indicate that biotite syenogranites (557 Ma) reflect a different magmatic event with respect to that giving rise to rhyolites and syenogranites (524.3±5.3 to 521.3±4.2 524 Ma, which are equivalent within error). These ages show

Table 4a. Whole rock Rb-Sr isotope data from Dehzaman biotite syenogranites and syenogranites. Analytical methods are described in Section 3.

Sample No.	Sr (ppm)	Rb (ppm)	$^{87}\text{Rb}/^{86}\text{Sr}$	$^{87}\text{Rb}/^{86}\text{Sr}$ Error (2s)	$(^{87}\text{Sr}/^{86}\text{Sr})_m$	$^{87}\text{Sr}/^{86}\text{Sr}$ Error (2s)	$(^{87}\text{Sr}/^{86}\text{Sr})_i$
Biotite syenogranite							
H26	100.3	117.8	3.406	0.096	0.732014	0.000023	0.705402
H31	74.4	139.6	5.450	0.150	0.745404	0.000022	0.702834
H33	82.1	123.7	4.370	0.120	0.738734	0.000027	0.704572
Syenogranite							
A12	57.6	65.5	3.298	0.093	0.731492	0.000023	0.707399
A13	75.6	49.6	1.901	0.054	0.721076	0.000019	0.707190
A18	145.2	75.4	1.504	0.043	0.718160	0.000023	0.707172
A29	110.8	78.0	2.040	0.058	0.721595	0.000025	0.706694

Table 4b. Whole rock Sm-Nd isotope data from Dehzaman biotite syenogranites and syenogranites. Analytical methods are described in Section 3.

Sample No.	Nd (ppm)	Sm (ppm)	$^{147}\text{Sm}/^{144}\text{Nd}$	$^{147}\text{Sm}/^{144}\text{Nd}$ Error (2s)	$(^{143}\text{Nd}/^{144}\text{Nd})_m$	$^{143}\text{Nd}/^{144}\text{Nd}$ Error (2s)	$(^{143}\text{Nd}/^{144}\text{Nd})_i$	ϵNd_i	TDM (Ga)
Biotite syenogranite									
H26	19.9	3.60	0.109	0.006	0.512280	0.000020	0.511881	-0.8	1.1
H31	16.1	3.08	0.116	0.006	0.512314	0.000012	0.511892	-0.6	1.1
H33	12.2	1.85	0.092	0.005	0.512226	0.000012	0.511891	-0.6	1.0
Syenogranite									
A12	0.9	0.18	0.121	0.017	0.512343	0.000031	0.511930	-0.7	1.2
A13	1.5	0.36	0.145	0.016	0.512353	0.000013	0.511857	-2.1	1.5
A18	1.9	0.41	0.131	0.015	0.512333	0.000019	0.511887	-1.6	1.3
A29	4.6	1.02	0.134	0.009	0.512332	0.000016	0.511874	-1.8	1.4

Figure 8. $(^{87}\text{Sr}/^{86}\text{Sr})_i$ vs ϵNd_i diagram for Dehzaman intrusive rocks. Data for Bornaward granites and Taknar granitoids are from Monazzami Bagherzadeh et al. (2015) and Shafaii Moghadam et al. (2017), respectively. Also, data for Mid-Ocean Ridge Basalts (MORB), Depleted Mantle (DM), Ocean-Island Basalts (OIB) and Island Arc Basalts (IAB) are from Zindler and Hart (1986). Initial ratios calculated for 557 and 521 Ma for biotite syenogranites and syenogranites, respectively.

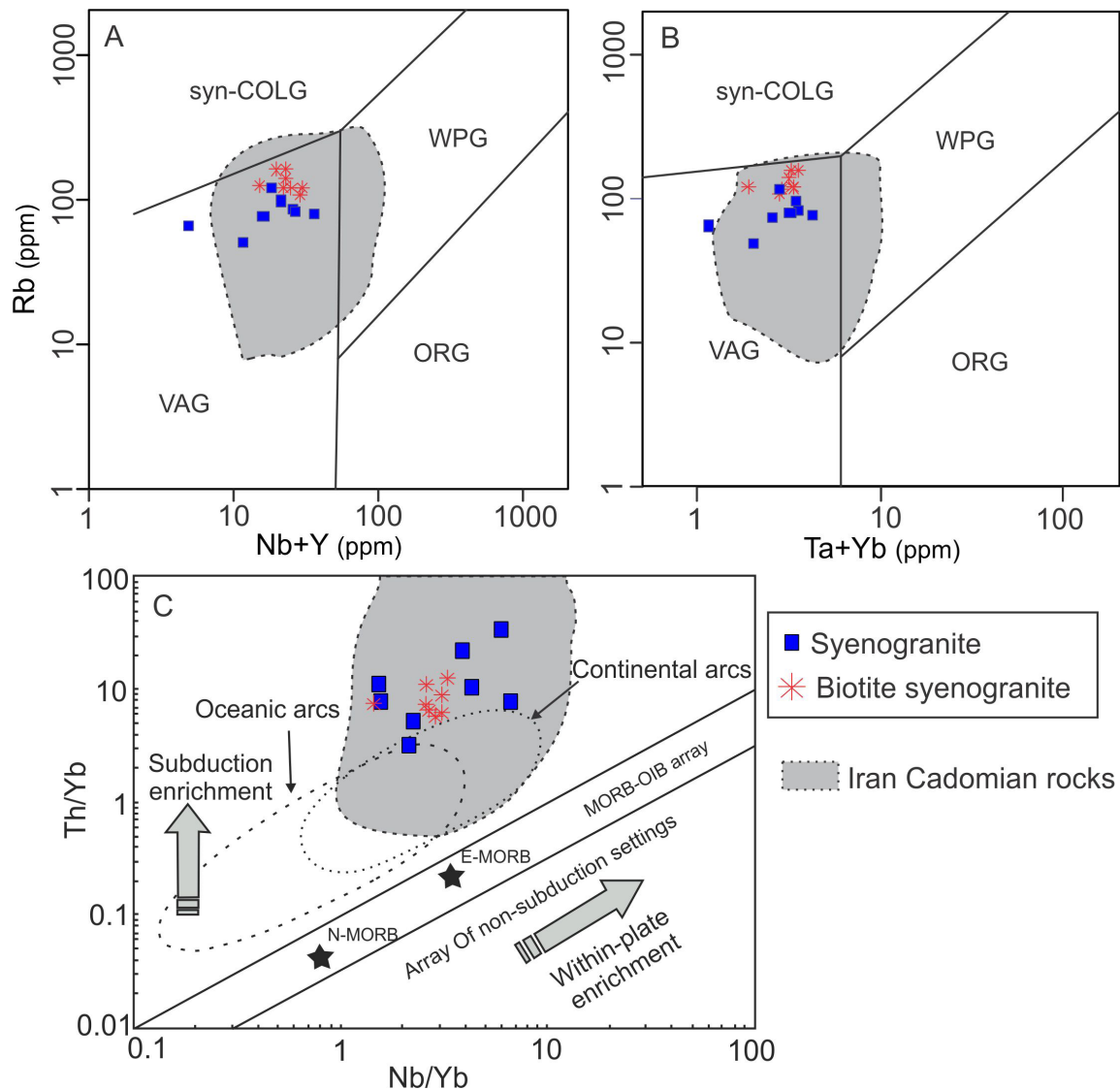


Figure 9. Tectonic discrimination diagrams for Dehzman intrusive rocks. (A) Rb vs Nb+Y, (B) Rb vs Ta+Yb, and (C) Th/Yb vs Nb/Yb (Modified after Perace et al., 1984 and Pearce, 2008). Data for Iran Cadomian rocks modified after Shafaii Moghadam et al. (2015), using other articles. N-MORB: Normal Mid-Ocean Ridge Basalts; E-MORB: Enriched Mid-Ocean Ridge Basalts; Syn-COLG: Syn-Collisional Granitoids; ORG: Ocean Ridge Granitoids; VAG: Volcanic Arc Granitoids; WPG: Within Plate Granitoids.

a prevalent magmatism, lasted for ~36 m.yr. in NE Iran, though more zircon U-Pb ages are needed to bracket this temporal variation.

The intrusive rocks are high-K calc-alkaline to shoshonitic and mainly peraluminous. They are also enriched in incompatible trace elements. The biotite syenogranites and syenogranites show slightly different petrographic (presence/absence of muscovite) and trace element geochemistry. Additionally, they have significantly different Sr-Nd isotopic composition, although, where overlapping Nd values are shown for the two granites.

Biotite syenogranites are characterized by variable initial $^{87}\text{Sr}/^{86}\text{Sr}$ ratio (<0.7054), low $\epsilon\text{Nd}(t)$ and negative Eu anomalies with $\text{Eu}/\text{Eu}^*=0.32-0.58$. Depletion in Eu, Ba, Sr, P, Nb and Ti seems to be related to highly fractionated nature of these rocks (Figure 6C). Whereas syenogranites are characterized by higher initial $^{87}\text{Sr}/^{86}\text{Sr}$ ratio (>0.7066), lower $\epsilon\text{Nd}(t)$, which have partly overlap with biotite syenogranites, and mostly positive Eu anomalies ($\text{Eu}/\text{Eu}^*=0.76-3.85$). Depletion in P, Nb and Ti are similar to biotite syenogranites, but Ba and Sr values are higher than (Figure 6D).

Negative Eu anomalies are related to the magma

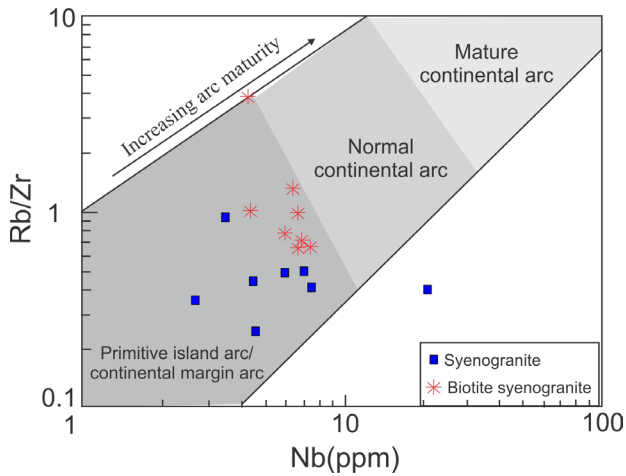


Figure 10. Rb/Zr vs Nb plot for Dehzaman intrusive rocks. Discrimination fields are from Brown et al. (1984).

differentiation including fractional crystallization of early K-feldspar and/or plagioclase (Henderson, 1984). However, under high fO_2 conditions, Eu mainly occurs as Eu^{3+} and only small amounts of Eu^{2+} are available for incorporation into plagioclase (Drake and Weill, 1975). These conditions (reduc or oxidation) can influence the Eu negative or positive anomalies as well. Positive Eu anomaly associated with Ba and Sr enrichment most likely also reflects a process of plagioclase accumulation (Borg et al., 1997; Leat et al., 2003).

Major and trace elements can be used to portrait

the fractionation trends of the Dehzaman rocks. For example, the negative Sr-Eu anomalies are controlled by the fractionation of plagioclase, whereas K-feldspar fractionation would produce negative Eu-Ba anomalies (Wu et al., 2003). Ba vs Sr and Ba/Sr vs Sr plots (Figure 11A and B) reveal the dependence of Sr concentration with Ba, which can be explained by the fractionation of plagioclase during the early stages of fractional crystallization of magmas and by the separation of plagioclase and biotite, rather than K-feldspar, during the late stages of melt fractionation. P depletion is also related to the apatite fractionation (Karen, 2002).

The negative anomalies in Nb and Ti can be explained by retention of these elements in Ti-rich residual mineral phases (i.e., rutile, titanite and ilmenite), either in the fractionating magmatic assemblages or in residual associations in the source area (Best, 2003; Rollinson, 1993). Ti can also be related to the fractional crystallization of titanium-bearing iron oxides in the shallow magma chambers.

To understand the age of the old continental crust involved during the assimilation, we calculated the Nd crustal residence age, TDM (The Depleted Mantel). The DePaolo (1981) model is used here, because it is more appropriate for calculating crustal extraction ages, generated in arc-like tectonic settings. The TDM ages obtained, vary between 1.0 and 1.5 Ga (Table 4b) suggesting that the oldest crustal component participated in the genesis of the studied magmatic rocks would have been separated from the mantle in the Mesoproterozoic or

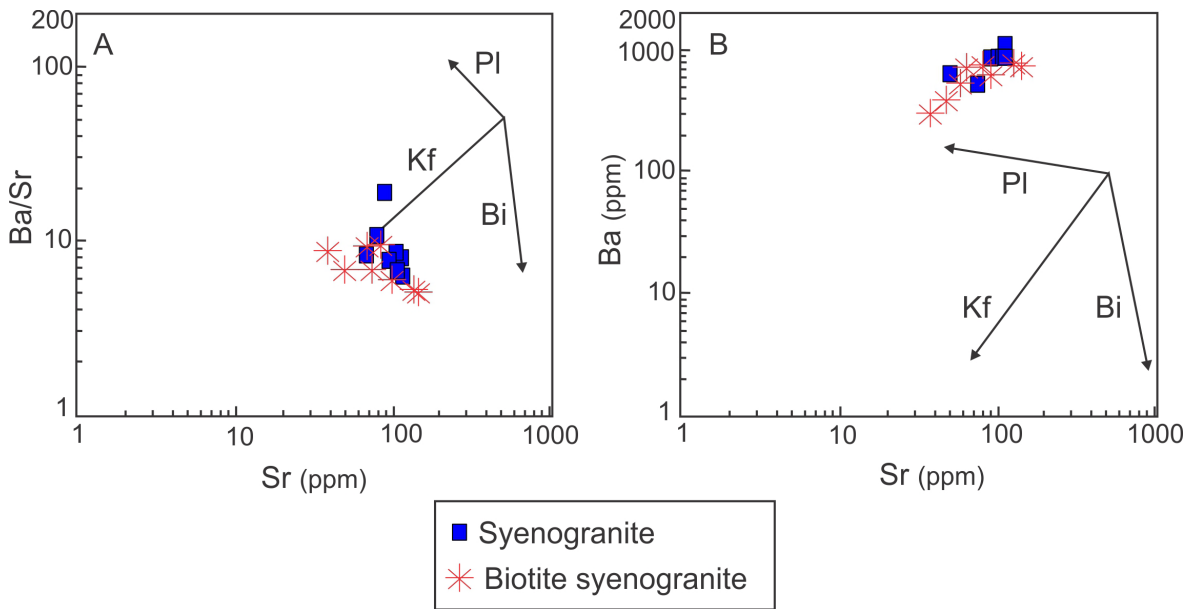


Figure 11. Ba/Sr vs Sr (A) and Ba vs Sr (B) diagrams for deciphering the fractionation trends of the granitic melts (modified after Hanson, 1978).

even in an older era.

The comparison of Sr-Nd isotopes of studied samples with Cadomian granites from the Bornaward and Taknar area in northern Dehzaman indicates good overlapping (Figure 8). The initial $^{87}\text{Sr}/^{86}\text{Sr}$ isotope values for the Bornaward granites range from 0.70351 to 0.7058 with $\varepsilon\text{Nd}(t)=-1.6$ to -3 (Monazzami Bagherzadeh et al., 2015), which are mostly similar to biotite syenogranites. The Bornaward granites yields a TDM age of 1.08-1.70 Ga (Monazzami Bagherzadeh et al., 2015). Taknar Cadomian granites have U-Pb zircon ages of ca 552-547 Ma. Rhyolites are coeval with the granites, with U-Pb zircon ages of ~ 551 Ma. Granodioritic dikes show two U-Pb zircon ages; ca 531 and 548 Ma. Geochemically, the Taknar igneous rocks have calc-alkaline signatures typical of continental arcs. The initial $^{87}\text{Sr}/^{86}\text{Sr}$ ($t=550$ Ma) of the Taknar Cadomian granitoids ranges between 0.705 and 0.711. Granitoids have particularly low $\varepsilon\text{Nd}(t)$ values (-0.5 to -4.0), which give depleted mantle model ages (TDM) of 1.7-1.3 Ga. Rhyolites and granodioritic dikes have $\varepsilon\text{Nd}(t)$ of -0.4 to -1.4 with TDM of ~ 1.3 -1.2 Ga (Shafaii Moghadam et al., 2017). Based on Sr-Nd isotopes, Taknar granitoids show higher contamination with continental crust than Dehzaman and Bornaward granites (Figure 8). Shafaii Moghadam et al. (2017) suggested Taknar complex, confirm that the magmatic rocks were generated via mixing of magmas with older continental crust components at an active continental margin.

To understand the petrogenetic characteristics of the Dehzaman granites we have used a series of major and trace elements discriminating diagrams. For example, in the FeO_t/MgO vs $10,000 \cdot \text{Ga}/\text{Al}$ and the Zr, Ce, and Nb vs $10,000 \cdot \text{Ga}/\text{Al}$ diagrams of Whalen et al. (1987), the intrusive rocks mainly plotted in the I- and S-type granites fields (Figure 12). However, some samples plot in the A-type granitic domain. A-type granites are usually distinguished by high $\text{FeO}_t/(\text{FeO}_t + \text{MgO})$ ratio, along with high Zr (commonly >300 ppm), HFSEs (especially Nb and Y), REE $^{3+}$, Ga, and Zn contents (Whalen et al., 1987). The Dehzaman intrusive rocks have low Zr (<300 ppm), Ce (<100 ppm), and Nb (<15 ppm), therefore, an A-type signature cannot be considered for the Dehzaman intrusive rocks. The high FeO_t/MgO ratio of some syenogranites shows slight supergene oxidation nature of these rocks during the alteration. The FeO content of these rocks are less than 2.6 wt%.

Mineralogical composition of granitoids, associated with their isotopic signatures, are powerful tools for distinguishing granitoids and their tectonic settings. For example I-type granites can contain ferromagnesian minerals like as amphibole and have quite low $^{87}\text{Sr}/^{86}\text{Sr}$ ratio; <0.708 . In contrast, S-type granites are peraluminous and can contain minerals such as garnet and alumina-

silicates, also the occurrence of components inherited by the sedimentary source material. The $^{87}\text{Sr}/^{86}\text{Sr}$ ratio of S-type granites is >0.708 to 0.717 (Chappell and White, 2001).

S-type granitic magmas are derived through partial melting of metasedimentary rocks that had a significant fraction of Al-rich clays in their protoliths. However, the origin of I-type granites has been and is in dispute (Clemens et al., 2011). Clemens et al. (2011) suggested there should be granitic rocks transitional between S- and I-type, depending on the balance between clay-rich and clay-poor rocks in the protolith. They believe melting of biotite+sillimanite assemblages will occur significantly earlier during a crustal heating cycle than will that of the hornblende+biotite assemblages that will predominate in I-type sources. Thus, even where interlayered sources do exist, S- and I-type magmas may be produced as temporally separate batches.

Although, Dehzaman granites have similarity with S-Type granites may be indicated by Al saturation index and presence of magmatic Al-rich minerals (e.g., white mica in biotite syenogranites), but also have low initial $^{87}\text{Sr}/^{86}\text{Sr}$ ratio (<0.707), with $\varepsilon\text{Nd}(t)$ values between -0.6 and -2.1 , which are typical of I-type granites. Furthermore, in the Na_2O vs K_2O diagram the Dehzaman granites fall in the field of granites with I-type affinities except one sample (Figure 13A). The Rb/Sr vs Rb/Ba diagram shows the Dehzaman granites plot next to metapsammite and metagreywacke derived melts and clay-poor in the protolith (Figure 13B).

SUMMARY AND CONCLUDING REMARKS

Subduction of proto-Tethyan oceanic lithosphere beneath northern Gondwana was responsible for arc magmatism during Ediacaran-Cambrian time (Figure 14). The Cadomian magmatism (ca. 599-500 Ma) is reported from Central Iran, Sanandaj-Sirjan Zone, NE Iran and even Alborz (Ramezani and Tucker, 2003; Hassanzadeh et al., 2008; Jamshidi Badr et al., 2013; Rossetti et al., 2015; Shafaii Moghadam et al., 2015; this study). The Cadomian magmatic rocks are also recorded from Turkey (570-530 Ma, Gürsu and Göncüoğlu, 2006; Okay et al., 2008; Ustaömer et al., 2005, 2009, 2012;), and from SW and central Europe, including Iberia and Bohemia (Genna et al., 2002; Murphy et al., 2002; Mushkin et al., 2003). The subduction seems to be started >600 Ma in Europe but the geochronological data support the subduction initiation at ~ 570 in eastern Gondwana including Turkey and Iran (Linnemann and Romer, 2002; Shafaii Moghadam et al., 2017). The subduction regime for the formation of the Cadomian arcs are ambiguous. Rossetti et al. (2015) suggested oblique subduction of the proto-Tethyan ocean beneath northern Gondwana to produce

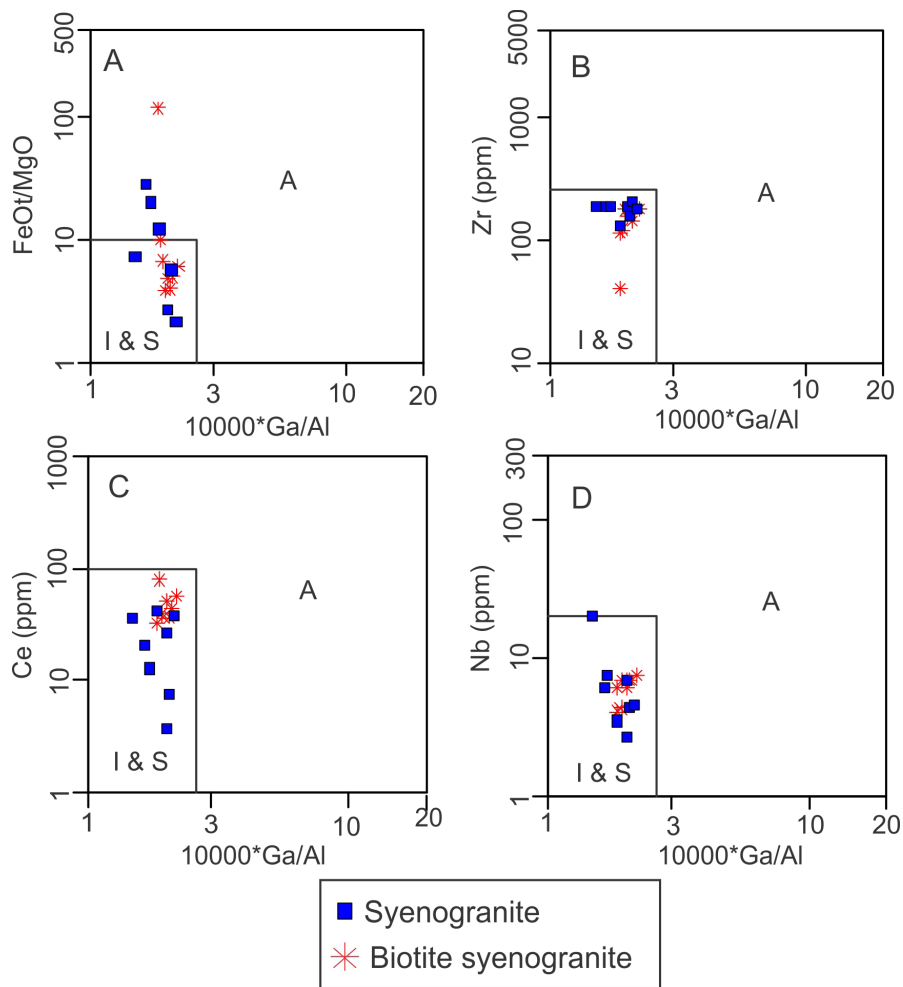


Figure 12. FeOt/MgO, Zr, Ce, and Nb vs $10,000 \cdot \text{Ga}/\text{Al}$ discrimination diagrams. (Modified after Whalen et al., 1987).

the Cadomian arcs.

This scenario can explain the dominance of extreme continental extension during late Neoproterozoic, which was responsible for a magmatic flare-up at that time (Shafaii Moghadam et al., 2017). Subduction beneath the northern Gondwana is suggested to have ceased around 450–400 Ma, due to continental or oceanic plateau collision (Ustaömer et al., 2009). However, geological evidence support epirogenic activity during 450–400 Ma, along with Palotethys rifting in N Gondwana (Shafaii Moghadam et al., 2015). This evidence includes deposition of a thick sequence of continental sediments in Iran and Anatolia during late Neoproterozoic-Cambrian and the eruption of Ordovician basaltic rocks with continental tholeiitic affinity in NE Iran (Derakhshani and Ghasemi, 2015).

Dehzaman igneous rocks including syenogranites and rhyolites with ages of 524.3 ± 5.3 Ma and 521.3 ± 4.2 Ma, respectively. These ages are quite younger than the age of biotite syenogranites (~ 557 Ma), obtained by Rossetti

et al. (2015). These ages related to late Neoproterozoic (Ediacaran) to early Cambrian. Geochemically, Dehzaman intrusive rocks have calcic-alkali to calc-alkalic and I-type signatures. These granites were derived from psammite and greywacke rocks and clay-poor in the protolith.

These rocks provide further evidence for the dominance of Cadomian magmatism in Iranian plateau. Geochemical data indicate these rocks formed during early stages of an active continental arc magmatism.

ACKNOWLEDGEMENTS

This study was supported by a grant from Research Foundation of Ferdowsi University of Mashhad (Iran) (Project No. 36972.3). We thank Mr. Naghipour, Maleki, Eatemadi, Shabani and Hashemi for helping during the field works. We acknowledge G. Gehrels and V. Valencia (University of Arizona) for their help during U-Pb zircon dating.

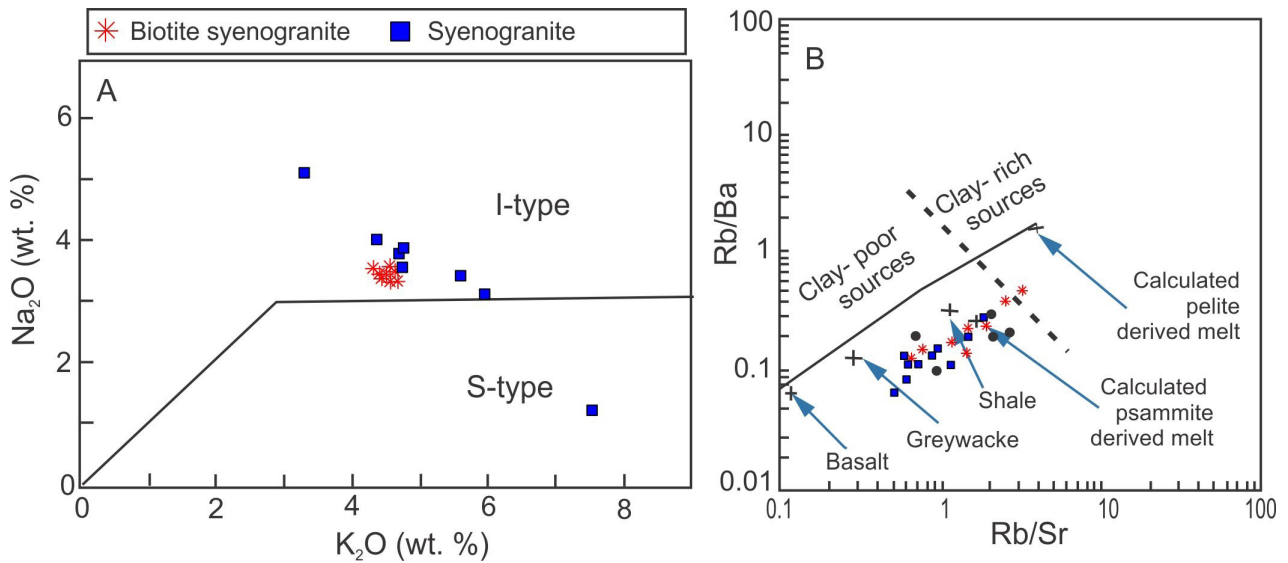


Figure 13. A. Na₂O vs K₂O plot to discriminates the Dehzman granites. I-type granites generally contain slightly higher Na₂O than S-type granites at the same K₂O content (Modified after Chappell and White, 2001). B. Plot of Rb/Sr vs Rb/Ba (Sylvester, 1998), the melt of Dehzman granites was derived from psammite and greywacke rocks.

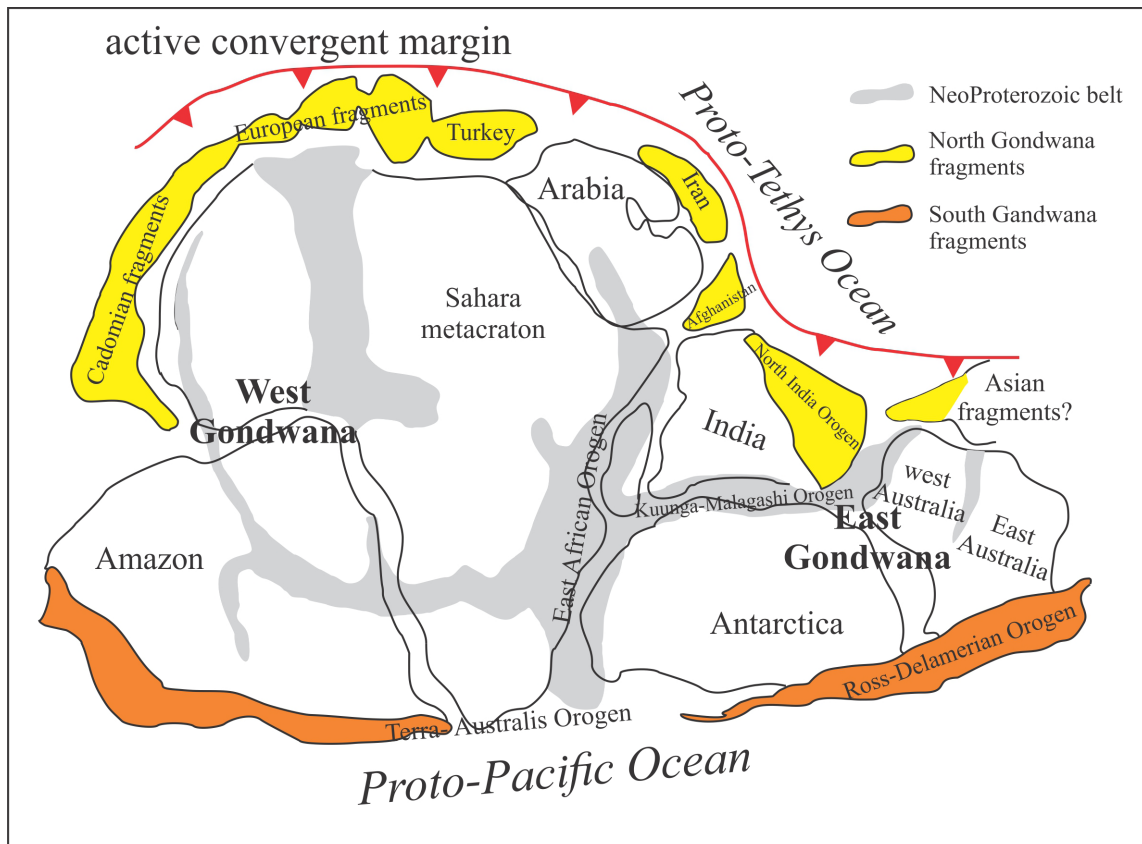


Figure 14. The configuration of the Gondwanan Supercontinent at 550 Ma. The Cadomian subduction system at the northern margin of Gondwana are also indicated (modified after Cawood et al., 2007; Shafaii Moghadam et al., 2015).

REFERENCES

- Alaminia Z., Karimpour M.H., Homam S.M., Finger F., 2013. The magmatic record in the Arghash region (northeast Iran) and tectonic implications. *International Journal of Earth Sciences* 10, 1603-1625.
- Alavi M., 1991. Tectonic map of the Middle East: Tehran. Geological Survey of Iran, scale 1:5,000,000.
- Altherr R., Topuz G., Siebel W., Sen C., Meyer H.P., Satir M., Lahaye Y., 2008. Geochemical and Sr-Nd-Pb isotopic characteristics of Paleocene plagioclinites from the Eastern Pontides (NE Turkey). *Lithos* 105, 149-161.
- Arslan M., Temizel T., Abdioglu E., Kolayli H., Yucel C., Boztug D., Sen C., 2013. ^{40}Ar - ^{39}Ar dating, whole-rock and Sr-Nd-Pb isotope geochemistry of postcollisional Eocene volcanic rocks in the southern part of the Eastern Pontides (NE Turkey): implications for magma evolution in extension-induced origin. *Contribution of Mineralogy and Petrology* 166, 113-142.
- Azizi H., Chung S.L., Tanaka T., Asahara Y., 2011. Isotopic dating of the Khoy metamorphic complex (KMC), northwestern Iran: a significant revision of the formation age and magma source. *Precambrian Research* 185, 87-94.
- Best M.G., 2003. *Igneous and Metamorphic Petrology*. Blackwell Publishing, 729 pp.
- Boari E., Avanzinelli R., Melluso L., Giordano G., Mattei M., De Benedetti A.A., Morra V., Conticelli S., 2009. Isotope geochemistry (Sr-Nd-Pb) and petrogenesis of leucite-bearing volcanic rocks from "Colli Albani" volcano, Roman Magmatic Province, Central Italy: inferences on volcano evolution and magma genesis. *Bulletin of Volcanology* 71, 977-1005.
- Boger S. and Miller J.M., 2004. Terminal suturing of Gondwana and the onset of the Ross-Delamerian Orogeny: the cause and effect of an Early Cambrian reconfiguration of plate motions. *Earth and Planetary Science Letters* 219, 35-48.
- Borg L.E., Clyne M.A., Bullen T.D., 1997. The variable role of slab-derived fluids in the generation of a suite of primitive calc-alkaline lavas from the southernmost Cascades, California. *The Canadian Mineralogist* 35, 425-452.
- Boynton W.V., 1984. Geochemistry of the rare earth elements: meteorite studies. In: *Rare Earth Element Geochemistry*. (Ed.): P. Henderson, Elsevier Science, Amsterdam (Netherlands), 63-114.
- Brown W.M., Kwak T., Askins P.W., 1984. Geology and geochemistry of an F-Sn-W skarn system - the Hole 16 deposit, Mt Garnet, North Queensland, Australia. *Australian Journal of Earth Science* 31, 317-340.
- Cawood P.A., 2005. Terra Australis Orogen: Rodinia breakup and development of the Pacific and Iapetus margins of Gondwana during the Neoproterozoic and Paleozoic. *Earth Science Review* 69, 249-279.
- Cawood P.A., Buchan C., 2007. Linking accretionary orogenesis with supercontinent assembly. *Earth Science Review* 82, 217-256.
- Cawood P.A., Johnson M.R.W., Nemchin A.A., 2007. Early Paleozoic orogenesis along the Indian margin of Gondwana. Tectonic response to Gondwana assembly. *Earth Planet Science Letter* 255, 70-84.
- Chappell B.W. and White A.J.R., 1974. Two contrasting granite types. *Pacific Geology* 8, 173-174.
- Chappell B.W. and White A.J.R., 2001. Two contrasting granite types: 25 years later. *Australian Journal of Earth Science* 48, 489-499.
- Cherniak D.J. and Watson E.B., 2001. Pb diffusion in zircon. *Chemical Geology* 172, 5-24.
- Clemens J.D., Stevens G., Farina F., 2011. The enigmatic sources of I-type granites: The peritectic connexion. *Lithos* 126, 174-181.
- Collins A.S. and Pisarevsky S.A., 2005. Amalgamating eastern Gondwana: the evolution of the circum-Indian orogens. *Earth-Science Reviews* 71, 229-270.
- Connelly J.N., 2001. Degree of preservation of igneous zonation in zircon as a signpost for concordancy in U/Pb geochronology. *Chemical Geology* 172, 25-39.
- Corfu F., Hanchar J.M., Hoskin P.W.O., Kinny P., 2003. Atlas of zircon textures. In: *Review of Mineralogy and Geochemistry*. (Eds.): J.M. Hanchar and P.W.O. Hoskin, Washington DC (USA), 469-500.
- Dalziel I.W.D., 1991. Pacific margins of Laurentia and East Antarctica-Australia as a conjugate rift pair: evidence and implications for an Eocambrian supercontinent. *Geology* 19, 598-601.
- DePaolo D.J., 1981. Trace element and isotopic effects of combined wall rock assimilation and fractional crystallization. *Earth and Planetary Science Letters* 53, 189-202.
- Dickin A.P., 2005. *Radiogenic Isotope Geology*. Press Syndicate of the University of Cambridge, London, 175 pp.
- Drake M.J., Weill D.F., 1975. Partition of Sr, Ba, Ca, Y, Eu^{2+} , Eu^{3+} , and other REE between plagioclase feldspar and magmatic liquid - experimental Study. *Geochimica et Cosmochim. Acta* 39, 689-712.
- Duggen S., Hoernle K., Van Den Bogaard P., Garbe-Schönberg D., 2005. Post-collisional transition from subduction- to intraplate-type magmatism in the westernmost Mediterranean: evidence for continental-edge delamination of subcontinental lithosphere. *Journal of Petrology* 46.
- Eftekharneshad J., Ruttner M.H., Valeh A., Alavi N., Hajian M., Haghypour J.A., 1977. Geological map of Ferdows (1:250000), Geological survey of Iran, Tehran (Iran).
- Frost B.R., Barnes G.G., Collins W.J., Arculus R.J., Ellis D.J., Frost C.D., 2001. A geological classification for granitic rocks. *Journal of Petrology* 42, 2033-2048.
- Foley S.F., Venturelli G., Green D.H., Toscani L., 1987. The ultrapotassic rocks: characteristics, classification, and constraints for petrogenetic models. *Earth Science Review* 24, 81-134.
- Gehrels G.E., Valencia V.A., Ruiz, J., 2008. Enhanced

- precision, accuracy, efficiency, and spatial resolution of U-Pb ages by laser ablation-multicollector-inductively coupled plasma-mass spectrometry. *Geochemistry, Geophysics and Geosystems* 9, 1-13.
- Gehrels G., Rusmore M., Woodsworth G., Crawford M., Andronicos C., Hollister L., Patchett J., Ducea M., Butler R., Klepeis K., Davidson C., Friedman R., Haggart J., Mahoney B., Crawford W., Pearson D., Girardi J., 2009. U-Th-Pb geochronology of the Coast Mountains batholith in north-coastal British Columbia: constraints on age and tectonic evolution. *Geological Society of American Bulletin* 121, 1341-1361.
- Genna A., Nehlig P., Le Goff E., Guerrot C., Shanti M., 2002. Proterozoic tectonism of the Arabian Shield. *PreCambrian Research* 117, 21-40.
- Gill J.B., 1981. *Orogenic Andesites and Plate Tectonics*. Springer, New York, 390 pp.
- Gürsu S. and Göncüoğlu M.C., 2006. Petrogenesis and tectonic setting of Cadomian felsic igneous rocks, Sandikli area of the western Taurides, Turkey. *International Journal of Earth Science* 95, 741-757.
- Gust D.A., Arculus R.A., Kersting A.B., 1997. Aspects of magma sources and processes in the Honshu arc. *The Canadian Mineralogist* 35, 347-365.
- Hanson G.N., 1978. The application of trace elements to the petrogenesis of igneous rocks of granitic composition. *Earth and Planetary Science Letter* 38, 26-43.
- Hassanzadeh J., Stockli D.F., Horton B.K., Axen G.J., Stockli L.D., Grove M., Schmitt A.K., 2008. U-Pb zircon geochronology of Late Neoproterozoic-Early Cambrian granitoids in Iran: implications for paleogeography, magmatism, and exhumation history of Iranian basement. *Tectonophysics* 451, 71-96.
- Henderson P., 1984. *Rare Earth Element Geochemistry*. Elsevier, Amsterdam (Netherlands), 510 pp.
- Horton B.K., Hassanzadeh J., Stockli D.F., Axen G.J., Gillis R.J., Guest B., Amini A., Fakhari M.D., Zamanzadeh S.M., Grove M., 2008. Detrital zircon provenance of Neoproterozoic to Cenozoic deposits in Iran: implications for chronostratigraphy and collisional tectonics. *Tectonophysics* 451, 97-122.
- Hu P., Li C., Wang M., Xie C., Wu Y., 2013. Cambrian volcanism in the Lhasa terrane, southern Tibet: record of an early Paleozoic Andean-type magmatic arc along the Gondwana proto-Tethyan margin. *Journal of Asian Earth Science* 77, 91-107.
- Jafari S.M., Shemirani A., Hamdi B., 2007. Microstratigraphy of the Late Ediacaran to Ordovician in NW Iran (Takab area). In: *The Rise and Fall of the Ediacaran Biota*. (eds): P. Vickers-Rich and P. Komarower, Geological Society of London 286, 433-437.
- Jamshidi Badr M., Collins A.S., Masoudi F., Cox G., Mohajjel M., 2013. The U-Pb age, geochemistry and tectonic significance of granitoids in the Soursat Complex, Northwest Iran. *Turkish Journal of Earth Science* 22, 1-31.
- Jiang Y.H., Jiang S.Y., Dai B.Z., Liao S.Y., Zhao K.D., Ling H.F., 2009. Middle to late Jurassic felsic and mafic magmatism in southern Hunan province, southeast China: implications for a continental arc to rifting. *Lithos* 107, 185-204.
- Karen R., Thomas A., Thomas W., 2002. Origin and emplacement of the andesite of Burroughs Mountain, a zoned, Large volume lava flow at Mount Rainier, Washington, USA. *Journal of Volcanology and Geothermal Research* 119, 275-296.
- Kemp A.I.S., Hawkesworth C.J., Foster G.L., Paterson B.A., Woodhead J.D., Hergt J.M., Gray C.M., Whitehouse M.J., 2007. Magmatic and crustal differentiation history of granitic rocks from hafnium and oxygen isotopes in zircon. *Science* 315, 980-983.
- Lam P.J., 2002. *Geology, geochronology, and thermochronology of the Alam Kuh area, central Alborz Mountains, northern Iran*. M.S. thesis, University of California, Los Angeles. 135 pp.
- Leat P.T., Smellie J.L., Millar I.L., Larter R.D., 2003. Magmatism in the South Sandwich arc. In: *Intra-Oceanic Subduction Systems: Tectonic and Magmatic Processes*. (Eds.): R.D. Larter and P.T. Leat, Geological Society of London 219, 285-313.
- Li Z.X., Bogdanova S.V., Collins A.S., Davidson A., DeWaele B., Ernst R.E., Fitzsimons I.C.W., Fuck R.A., Gladkochub D.P., Jacobs J., Karlstrom K.E., Lu S., Natapov L.M., Pease V., Pisarevsky S.A., Thrane K., Vernikovsky V., 2008. Assembly, configuration, and break-up history of Rodinia: a synthesis. *PreCambrian Research* 160, 179-210.
- Li X.H., Li W.X., Wang X.C., Li Q.L., Liu Y., Tang G.Q., 2009. Role of mantle derived magma in genesis of early Yanshanian granites in the Nanling Range, South China: in situ zircon Hf-O isotopic constraints. *Science China Earth Science* 52, 1262-1278.
- Ludwig KR., 2003. *ISOPLOT 3.0: A Geochronological Toolkit for Microsoft Excel*. Special Publication, Berkeley Geochronology Center, California, 74 pp.
- Ma L., Jiang S., Hou M., Dai B., Jiang Y., Yang T., Zhao K., Wie P., Zhu Z., Xu B., 2014. Geochemistry of early cretaceous calc-alkaline lamprophyres in the Jiaodong Peninsula: implication for lithospheric evolution of the eastern North China craton. *Gondwana Research* 25, 859-872.
- Mahmoud R.I., Faryad S.W., Holub F.V., Košler J., Frank W., 2011. Magmatic and metamorphic evolution of the Shotur Kuh metamorphic complex (Central Iran). *International Journal of Earth Science* 100, 45-62.
- Maniar P.D. and Piccoli P.M., 1989. Tectonic discrimination of granitoids. *Geological Society of American Bulletin* 101, 635-643.
- Middlemost E.A.K., 1994. Naming materials in the magma/igneous rock system. *Earth Science Review* 37, 215-224.
- Monazzami Bagherzadeh R., Karimpour M.H., Lang Farmer G.,

- Stern C.R., Santos J.F., Rahimi B., Heidarian Shahri M.R., 2015. U-Pb zircon geochronology, petrochemical and Sr-Nd isotopic characteristic of Late Neoproterozoic granitoid of the Bornaward Complex (Bardaskan-NE Iran). *Journal of Asian Earth Science* 111, 54-71.
- Murphy J.B., Eguiluz L., Zulauf G., 2002. Cadomian orogens, peri-Gondwanan correlatives and Laurentia-Baltica connections. *Tectonophysics* 352, 1-9.
- Murphy J.B., Pisarevsky S.A., Nance R.D., Keppie J.D., 2004. Neoproterozoic Early Paleozoic evolution of peri-Gondwanan terranes: implications for Laurentia-Gondwana connections. *International Journal of Earth Science* 93, 659-682.
- Mushkin A., Navon O., Halicz L., Hartmann G., Stein M., 2003. The petrogenesis of A type magmas from the Amram massif, Southern Israel. *Journal of Petrology* 44, 815-832.
- Nance R.D., Murphy J.B., Strachan R.A., Keppie J.D., Gutiérrez-Alonso G., Fernández-Suárez J., Quesada C., Linnemann U., D'Lemos R., Pisarevsky S.A., 2008. Neoproterozoic-early Paleozoic tectonostratigraphy and palaeogeography of the peri-Gondwanan terranes: Amazonian v. West African connection. In: *The Boundaries of the West African Craton*. (Eds.): N. Ennih and J.P. Liégeois, Geological Society of London 297, 345-383.
- Nance R.D., Gutierrez Alonso G., Keppie J.D., Linnemann U., Murphy J.B., Quesada C., Strachan R.A., Woodcock N., 2010. Evolution of the Rheic Ocean. *Gondwana Research* 17, 194-222.
- Nance R.D., Murphy J.D., Santosh M., 2014. The supercontinent cycle: a retrospective essay. *Gondwana Research* 25, 4-29.
- Nutman A.P., Mohajjel M., Bennet V.C., Fergusson C.L., 2014. Gondwanan Eoarchean-Neoproterozoic ancient crustal material in Iran and Turkey: zircon U-Pb-Hf isotopic evidence. *Canadian Journal of Earth Science* 51, 272-285.
- Nozaem R., Mohajjel M., Rossetti F., Della Seta M., Vignaroli G., Yassaghi A., Salvini, S., Eliassi M., 2013. Post-Neogene right-lateral strike-slip tectonics at the north-western edge of the Lut Block (Kuh-e-Sarhangi Fault), Central Iran. *Tectonophysics* 589, 220-233.
- Okay A.I., Bozkurt E., Satir M., Yigitbas E., Crowley Q.G., Shang C.K., 2008. Defining the southern margin of Avalonia in the Pontides: geochronological data from the Late Proterozoic and Ordovician granitoids from NW Turkey. *Tectonophysics* 461, 252-264.
- Pearce J.A., Harris N.B.W., Tindle A.G., 1984. Trace element discrimination diagrams for the tectonic interpretation of granitic rocks. *Journal of Petrology* 25, 956-983.
- Pearce J.A. and Peate D.W., 1995. Tectonic implications of the composition of volcanic arc magmas. *Annual Review of Earth and Planetary Science* 23, 251-285.
- Pearce J.A., 2008. Geochemical fingerprinting of oceanic basalts with applications to ophiolite classification and the search for Archean oceanic crust. *Lithos* 100, 14-48.
- Peccerillo A. and Taylor S.R., 1976. Geochemistry of Eocene calc-alkaline volcanic rocks from the Kastamonu area (northern Turkey). *Contribution to Mineralogy and Petrology* 58, 63-81.
- Ramezani J. and Tucker R., 2003. The Saghand region, central Iran: U-Pb geochronology, petrogenesis and implication for Gondwana tectonics. *American Journal of Science* 303, 622-665.
- Rollinson H.R., 1993. *Using Geochemical Data: Evaluation, Presentation, Interpretation*. Longman Science and Technical 352 pp.
- Rossetti F., Nozaem R., Lucci F., Vignaroli G., Gerdes A., Nasrabadi M., Theye T., 2015. Tectonic setting and geochronology of the Cadomian magmatism in Central Iran, Kuh-e- Sarhangi region (NW Lut Block). *Journal of Asian Earth Science* 102, 24-44.
- Geological Survey of Iran, 1970. Ozbak Kuh mountain, Geological map, 1:100,000. Geological survey of Iran, Tehran (Iran).
- Geological Survey of Iran, 2011. Ghasemabad, Geological map, 1:100,000. Geological Survey of Iran, Tehran (Iran).
- Saki A., 2010. Proto-Tethyan remnants in northwest Iran: geochemistry of the gneisses and metapelitic rocks. *Gondwana Research* 17, 704-714.
- Shafaii Moghadam H., Khademi M., Hu Z., Stern R.J., Santos J.F., Wu Y., 2015. Cadomian (Ediacaran-Cambrian) arc magmatism in the ChahJam-Biarjmand metamorphic complex (Iran): Magmatism along the northern active margin of Gondwana. *Gondwana Research* 27, 439-452.
- Shafaii Moghadam H., Li X.H., Santos J.F., Stern R.J., Griffin W.L., Ghorbani G., Sarebani N., 2017. Neoproterozoic magmatic flare-up along the N. margin of Gondwana: The Taknar complex, NE Iran. *Earth and Planetary Science Letters* 478, 83-96.
- Stampfli G.M., Von Raumer J., Borel G., 2002. The Paleozoic evolution of pre Variscan terranes: from Gondwana to the Variscan collision. *Geological Society of America* 364, 263-280.
- Stocklin J., Ruttner A. and Nabavi M., 1964. New data on the Lower Paleozoic and pre-Cambrian of North Iran. *Geological Survey of Iran Report* (1), Tehran, Iran, 29 pp.
- Stocklin J. and Setudehnia A., 1977. *Stratigraphic Lexicon of Iran* (2nd edition). Geological Survey of Iran Report (18), Tehran, Iran, 376 pp.
- Sun S.S., McDonough W.F., 1989. Chemical and isotopy systematics of oceanic basalts: implications for mantle composition and processes. In: *Magmatism in the Ocean: Basins*. (Eds.): A.D. Saunders and M.J. Norry, Geological Society of London 42, 313-345.
- Sylvester P.J., 1998. Post-collisional strongly peraluminous granites. *Lithos* 45, 29-44.
- Tatsumi Y. and Takahashi T., 2006. Operation of subduction factory and production of andesite. *Journal of Mineralogical and Petrological Science* 101, 145-153.

- Torsvik T.H. and Cocks L.R.M., 2013. Gondwana from top to base in space and time. *Gondwana Research* 24, 999-1030.
- Ustaömer P.A., Mundil R., Renne P.R., 2005. U/Pb and Pb/Pb zircon ages for arc-related intrusions of the Bolu Massif (W Pontides, NW Turkey): evidence for Late PreCambrian (Cadomian) age. *Terra Nova* 17, 215-223.
- Ustaömer P.A., Ustaömer T., Collins A.S., Robertson A.H.F., 2009. Cadomian (Ediacaran-Cambrian) arc magmatism in the Bitlis Massif, SE Turkey: magmatism along the developing northern margin of Gondwana. *Tectonophysics* 473, 99-112.
- Ustaömer P.A., Ustaömer T., Gerdes A., Zulauf G., 2011. Detrital zircon ages from a Lower Ordovician quartzite of the Istanbul exotic terrane (NW Turkey): evidence for Amazonian affinity. *International Journal of Earth Science* 100, 23-41.
- Ustaömer P.A., Ustaömer T., Robertson A.H.F., 2011. Ion probe U-Pb dating of the Central Sakarya basement: a peri-Gondwana terrane intruded by Late Lower Carboniferous subduction/collision-related granitic rocks. *Turkish Journal of Earth Science* 21, 905-932.
- Villa I.M., De Bièvre P., Holden N.E., Renne P.R., 2015. IUPAC-IUGS recommendation on the half life of ^{87}Rb . *Geochimica et Cosmochimica Acta* 164, 382-385.
- Walker J.A., Patino L.C., Carr M.J., Feigenson M.D., 2001. Slab control over HFSE depletions in central Nicaragua. *Earth Planet of Science Letter* 192, 533-543.
- Wang B., Faure M., Cluzel D., Shu L.S., Charvet J., Meffre S., Ma Q., 2006. Late Paleozoic tectonic evolution of the northern West Chinese Tianshan Belt. *Geodinamica Acta* 19, 237-247.
- Whalen J.B., Currie K.L., Chappell B.W., 1987. A-type granites: geochemical characteristics, discrimination and petrogenesis. *Contribution of Mineralogy and Petrology* 95, 407-419.
- Whitney D.L. and Evans B.W., 2010. Abbreviations for names of rock-forming minerals. *American Mineralogist* 95, 185-187.
- Woodhead J., Eggins S., Gamble J., 1993. High field strength and transition element systematics in island arc and back-arc basin basalts: evidence for multi-phase melt extraction and a depleted mantle wedge. *Earth Planetary of Science Letter* 114, 491-504.
- Wu F.Y., Jahn B.M., Wilde S.A., Lo C.H., Yui T.F., Lin Q., Ge W.C., Sun D.Y., 2003. Highly fractionated I-type granites in NE China (II): isotopic geochemistry and implications for crustal growth in the Phanerozoic. *Lithos* 67, 191-204.
- Zhu D.C., Zhao Z.D., Niu Y.L., Dilek Y., Wang Q., Ji W.H., Dong G.C., Sui Q.L., Liu Y.S., Yuan H.L., Mo X.X., 2012. Cambrian bimodal volcanism in the Lhasa Terrane, southern Tibet: record of an early Paleozoic Andean-type magmatic arc in the Australian proto-Tethyan margin. *Chemical Geology* 328, 290-308.
- Zindler A. and Hart S.R., 1986. Chemical geodynamics. *Annual Review of Earth and Planetary Sciences* 14, 493-571.



This work is licensed under a Creative Commons Attribution 4.0 International License CC BY. To view a copy of this license, visit <http://creativecommons.org/licenses/by/4.0/>